Control of the T Follicular Helper–Germinal Center B-Cell Axis by CD8+ Regulatory T Cells Limits Atherosclerosis and Tertiary Lymphoid Organ Development

Marc Clement, PhD; Kevin Guedj, PhD; Francesco Andreata, MSc; Marion Morvan, MSc; Laetitia Bey, MSc; Jamila Khallou-Laschet, PhD; Anh-Thu Gaston, MSc; Sandrine Delbosc, PhD; Jean-Marc Alsac, MD, PhD; Patrick Bruneval, MD, PhD; Catherine Deschildre, MSc; Marie Le Borgne, PhD; Yves Castier, MD, PhD; Hye-Jung Kim, PhD; Harvey Cantor, MD, PhD; Jean-Baptiste Michel, MD, PhD; Giuseppina Caligiuri, MD, PhD; Antonino Nicoletti, PhD

Background—The atheromodulating activity of B cells during the development of atherosclerosis is well documented, but the mechanisms by which these cells are regulated have not been investigated.

Methods and Results—Here, we analyzed the contribution of Qa-1–restricted CD8+ regulatory T cells to the control of the T follicular helper–germinal center B-cell axis during atherogenesis. Genetic disruption of CD8+ regulatory T cell function in atherosclerosis-prone apolipoprotein E knockout mice resulted in overactivation of this axis in secondary lymphoid organs, led to the increased development of tertiary lymphoid organs in the aorta, and enhanced disease development. In contrast, restoring control of the T follicular helper–germinal center B-cell axis by blocking the ICOS-ICOSL pathway reduced the development of atherosclerosis and the formation of tertiary lymphoid organs. Moreover, analyses of human atherosclerotic aneurysmal arteries by flow cytometry, gene expression analysis, and immunofluorescence confirmed the presence of T follicular helper cells within tertiary lymphoid organs.

Conclusions—This study is the first to demonstrate that the T follicular helper–germinal center B-cell axis is proatherogenic and that CD8+ regulatory T cells control the germinal center reaction in both secondary and tertiary lymphoid organs. Therefore, disrupting this axis represents an innovative therapeutic approach. **(*Circulation*. 2015;131:560-570. DOI: 10.1161/CIRCULATIONAHA.114.010988.)**

Key Words: atherosclerosis ■ inflammation ■ leukocytes

The role of B cells in atherogenesis is currently being debated. T-independent innate-like B cells and the natural antibodies that they produce might be endowed with atheroprotective properties,[1,2] whereas T-dependent B cells have proatherogenic potential.[3,4] A major feature of these T-dependent B cells is that the antibodies they produce result from heavy-chain class switching and affinity maturation. These events occur in germinal centers (GCs) within secondary lymphoid organs but can also occur in tertiary lymphoid organs (TLOs). TLOs are formed in tissues subjected to chronic inflammation[5] such as atherosclerotic arteries because B-cell lymphoid follicles are present in the adventitial layer of these arteries.[6–10] However, B-cell activation and differentiation into memory or plasma cells require help from T follicular helper (Tfh) cells.[11] This process is a critical checkpoint in the adaptive immune response because, when crossed, the production of potentially self-reactive affinity-matured specific antibodies can be triggered for the life span of the organism. Consequently, Tfh cells must be finely regulated to avoid the overactivation or differentiation of B cells and the development of autoimmune pathologies, a regulatory task that may be allotted to Qa-1–restricted CD8+ regulatory T cells (CD8+ Tregs).

Editorial see p 525
Clinical Perspective on p 570

CD8+ Tregs are known to be critical gatekeepers for the control of autoreactive CD4+ T cells.[12–16] Previously unsuspected cell targets of CD8+ Tregs are Tfh cells because of their high basal expression of the Qa-1 molecule,[14] which is the mouse ortholog of the HLA-E molecule. The Qa-1 molecule can

Received May 10, 2014; accepted November 26, 2014.

From Unité 1148, Institut National de la Santé et de la Recherche Médicale (INSERM), Hôpital X Bichat, Paris, France (M.C., K.G., F.A., M.M., J.-K.L., A.-T.G., S.D., C.D., M.L.B., Y.C., J.-B.M., G.C., A.N.); Université Denis Diderot, Paris VII, Paris, France (M.C., K.G., F.A., L.B., J.-K.L., M.L.B., A.N.); Hôpital Européen Georges Pompidou, AP-HP, Faculté de Médecine René Descartes, Université Paris 5, Paris, France (J.-M.A., P.B.); and Department of Pathology, Harvard Medical School, Boston, MA (H.-J.K., H.C.).

The online-only Data Supplement is available with this article at http://circ.ahajournals.org/lookup/suppl/doi:10.1161/CIRCULATIONAHA.114.010988/-/DC1.

Correspondence to Antonino Nicoletti, PhD, INSERM UMRS1148 "Laboratory for Vascular Translational Science," X Bichat-C Bernard Hospital, 46 Rue Henri Huchard, 75018 Paris, France. E-mail antonino.nicoletti@inserm.fr

establish 2 types of molecular interactions: One with T cell receptors (TCRs) on CD8+ Tregs and the other with NKG2A receptors on CD8+ T cells and natural killer cells.[17]

To discriminate between the effects caused by NKG2A signaling and those resulting from TCR signaling, we used a transgenic mouse strain in which a point mutation was inserted into the Qa-1 molecule (D227K), thereby specifically abrogating its interaction with the TCR of CD8+ Tregs.[14]

By crossing the D227K mice with atherosclerosis-prone apolipoprotein E–knockout (ApoE°) mice, we could study how the control of the Tfh-GC B-cell axis by CD8+ Tregs affects the development of atherosclerosis. In parallel, we could comprehensively characterize Tfh cells in human atherothrombotic aortas. These studies clearly identify Tfh cells as key regulators of the proatherogenic B-cell responses.

Methods

Human Tissues

Abdominal aortic aneurysm (AAA) tissues were obtained from patients undergoing surgery and enrolled in the RESAA (REflet Sanguin de l'evolutivité des Anevrysmes de l'aorte abdominale) protocol. All patients gave written informed consent, and the protocol was approved by the Comite Consultatif de Protection des Personnes dans la Recherche Biomédicale (Paris-Cochin, approval No. 2095). Only noninflammatory AAAs with documented atheroma were selected for our studies. Control aortas were sampled from dead organ donors with the authorization of the French Biomedicine Agency (PFS 09-007). These control aortic samples were nonaneurysmal (N-AA) and devoid of thrombi but could present early atheromatous lesions.

Mice

ApoE° mice were purchased from the Jackson Laboratory, and generation of the Qa-1° and D227K (Qa-1$^{D227K/D227K}$) mice was described previously.[17,18] The experimental protocol was approved by the Animal Ethics Committee of the Institut National de la Santé et de la Recherche Médicale and was therefore performed in accordance with the ethics standards detailed in the 1964 Declaration of Helsinki and its later amendments. Review and approval of the study were also obtained from the Comité d'Éthique Paris-Nord #121 (No. B 7518 03). The groups of mice used, the treatment to which they were subjected, and the biochemical analyses performed on their blood are described in the online-only Data Supplement.

Cell and Tissue Analyses

Atherosclerotic lesions were measured as previously described.[1] Human and mouse tissues were characterized by immunohistochemistry. Cell suspensions were analyzed by flow cytometry. Please refer to the online-only Data Supplement for the detailed methods.

Adoptive Cell Transfer

The protocols used to transfer CD4+ T cells and CD8+ Tregs are described in the online-only Data Supplement.

Gene Expression Analysis

Total RNA extracted from cells sorted from human aortas was analyzed by real-time polymerase chain reaction, as described in the online-only Data Supplement.

Statistical Analysis

Statistical analyses were performed with the JMP9 and Prism software programs. Differences between groups were considered to be statistically significant when $P<0.05$ using the appropriate tests. We used Student *t* tests or 2-way ANOVA tests followed by Tukey post hoc tests when values were normally distributed or nonparametric Mann–Whitney tests when values were not normally distributed or when the population size was too small (n<8), as specified in the figure legends. Aortic B-cell cluster incidence was analyzed by use of a log-rank test.

Results

Expansion of Tfh and GC B Cells During Atherosclerosis Development

We first asked whether the Tfh cell population is modulated during atherosclerosis development and therefore compared the spleen cells of young (6 weeks old; n=3) and aged (40 weeks old; n=4) ApoE° mice. In the ApoE° mice, aging did not modify the overall percentage of CD4+ T cells (Figure 1A). However, the proportion of activated memory (CD44^{high}PD-1+) CD4+ T cells was dramatically increased in the aged mice compared with the young mice. Among these cells, the proportion of Tfh cells (ICOS+CXCR5+) was significantly increased (Figure 1A and 1B). The proportion of CD8+ T cells was also significantly increased in the aged mice. In contrast, the CD44^{high}CD122+Ly49+CXCR5+CD8+ T-cell population, in which CD8+ Tregs are enriched,[15] was sharply reduced, resulting in a dramatic increase in the Tfh cell/CD8+ Treg ratio (Figure 1A and 1B). Concomitantly, the aged ApoE° mice displayed a reduced percentage of splenic B cells (B220+), whereas the percentage of GC B cells significantly increased (Figure 1A and 1B). This observation was not reproduced in 40-week-old wild-type mice (data not shown), indicating that the effect is related to hypercholesterolemia and not to aging. Furthermore, the increased GC B-cell compartment was associated with increased immunoglobulin titers in the plasma of aged ApoE° mice (Figure IA in the online-only Data Supplement).

These data suggest that atherogenesis in ApoE° mice is characterized by defective Tfh cell regulation by CD8+ Tregs and the mirrored expansion of GC B cells.

CD8+ Tregs Control Tfh Cells in ApoE° Mice

To control the Tfh-GC B-cell axis in ApoE° mice, 40-week-old ApoE° mice were injected with cell suspensions enriched in CD8+ Tregs (n=3; CD44^{high}CD122+) or in memory CD8+ T cells (n=3; CD44^{high}CD122−) prepared from young (10 weeks old) ApoE° mice (Figure IB in the online-only Data Supplement). Transfer of the CD8+ Tregs significantly reduced the percentage of Tfh cells in the recipient mice 8 days after the injection compared with transfer of the memory CD8+ T cells, whereas the size of the pools of CD4+ and CD8+ T cells remained steady (Figure 1C and 1D). The specific effect observed on the Tfh cells was likely related to their higher expression of the Qa-1 molecule compared with naïve, memory, and regulatory CD4+ T cells (Figure IC in the online-only Data Supplement).

Qa-1–Restricted CD8+ Tregs Control Atherosclerosis Development in ApoE° Mice

To assess whether the CD8+ Tregs act through a TCR/Qa-1 interaction, ApoE° mice were crossed with Qa-1° mice or D227K mice.

Fatty streak lesions had similar sizes in the 3 groups at 8 weeks of age (n=12 ApoE°, n=7 ApoE°–Qa-1°, n=16

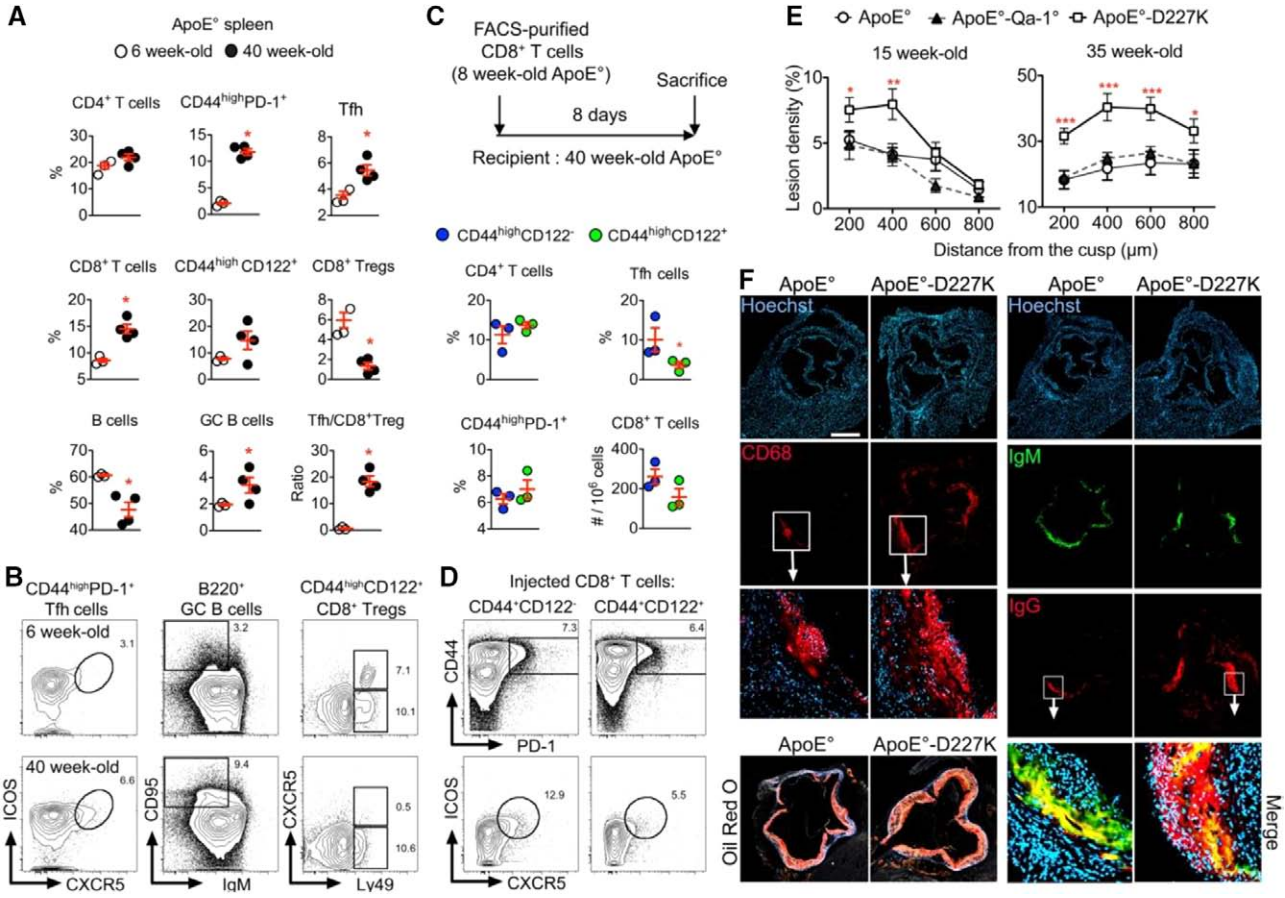

Figure 1. CD8+ regulatory T cells (Tregs) reduce atherogenesis and control the T follicular helper (Tfh)–germinal center (GC) B-cell axis in apolipoprotein E–knockout (ApoE°) mice. **A** and **B**, Flow cytometry analysis of total CD4+ T cells (among CD45+ cells), CD44highPD-1+ T cells (among CD4+ T cells), total CD8+ T cells (among CD45+ cells), CD44highCD122+ T cells (among CD8+ T cells), Ly49+CXCR5+ CD8+ Treg cells (among CD44highCD122+ cells), B220+ B cells (among CD45+ cells), CD95highIgMlow GC B cells (among B220+ B cells), and Tfh cells (among CD44highPD-1+ T cells) performed on the splenocytes from 6- (n=3) and 40- (n=4) week-old ApoE° mice. **C**, Quantification and (**D**) contour plot of CD4+ T cells (among CD45+ cells), CD44highPD-1+ T cells (among CD4+ T cells), and Tfh cells (among CD44highPD-1+ T cells) and the number of CD8+ T cells in the spleen of 40-week-old ApoE° mice (n=3) infused 8 days earlier with memory (CD44highCD122−; blue) or regulatory (CD44highCD122+; green) CD8+ T cells. **E**, Atherosclerotic lesions measured by the morphometric quantitative analysis of Oil Red O–stained aortic root cryosections from 15- and 35-week-old ApoE° (n=13 and n=12), ApoE°–Qa-1 (n=10 and n=10), and ApoE°-D227K mice (n=14 and n=9). **F**, Immunofluorescence analysis of aortic root cryosections from ApoE° and ApoE°-D227K mice stained for CD68 or IgM and IgG and nuclei (Hoechst). The white square boxes represent the areas magnified below. **Bottom left**, representative image of Oil Red O–stained aortic roots from ApoE° and ApoE°-D227K mice (scale bar, 500 µm). FACS indicates fluorescence-activated cell sorter. **P*<0.05, ***P*<0.01, ****P*<0.001, Mann–Whitney test (**A**, **C**) and 2-way ANOVA (**E**).

ApoE°-D227K; Figure IE in the online-only Data Supplement). However, the ApoE°-D227K mice (n=14 and n=9) developed significantly bigger plaques than did the ApoE° (n=13 and n=12) and ApoE°-Qa-1° (n=10 and n=10) mice at 15 and 35 weeks of age (Figure 1E and Figure ID in the online-only Data Supplement). Additionally, the plaques of the 35-week-old ApoE°-D227K mice displayed more intense CD68, vascular cell adhesion molecule-1, and IgG staining than did the 2 other strains, whereas IgM staining was similar among the 3 groups (Figure 1F and Figure ID in the online-only Data Supplement).

Therefore, loss of the regulation of Tfh cells by CD8+ Tregs enhanced the deposition of IgG-switched antibodies in plaques, which may have promoted a more inflammatory plaque environment and accelerated atherogenesis in ApoE°-D227K mice. ApoE°–Qa-1° and ApoE° mice yielded similar results because abrogating TCR (activating) and NKG2A (inhibitory) signaling in Qa-1° mice resulted in a composite "immune-neutral" phenotype as the result of the selection and function of CD8+ Treg cells being compromised and the activated CD4+ effector T cells being no longer protected against natural killer lysis. Consequently, most of the following studies were pursued with ApoE°-D227K mice.

Impaired CD8+ Treg Function Leads to Tfh and GC B-Cell Expansion

The aforementioned results indicate that B-cell responses are exaggerated in ApoE°-D227K mice. In support of this finding, 35-week-old ApoE°-D227K mice (n=4) displayed a significantly increased proportion of splenic Tfh cells compared with age-matched ApoE° mice (n=5; Figure 2A), which was likely attributable to their high expression of Bcl6 (Figure IIA and IIB in the online-only Data Supplement) and their high proliferation rate (Figure IIC in the online-only Data Supplement). Accordingly, the percentage of GC B cells was increased in ApoE°-D227K mice (Figure 2B), whereas the percentages

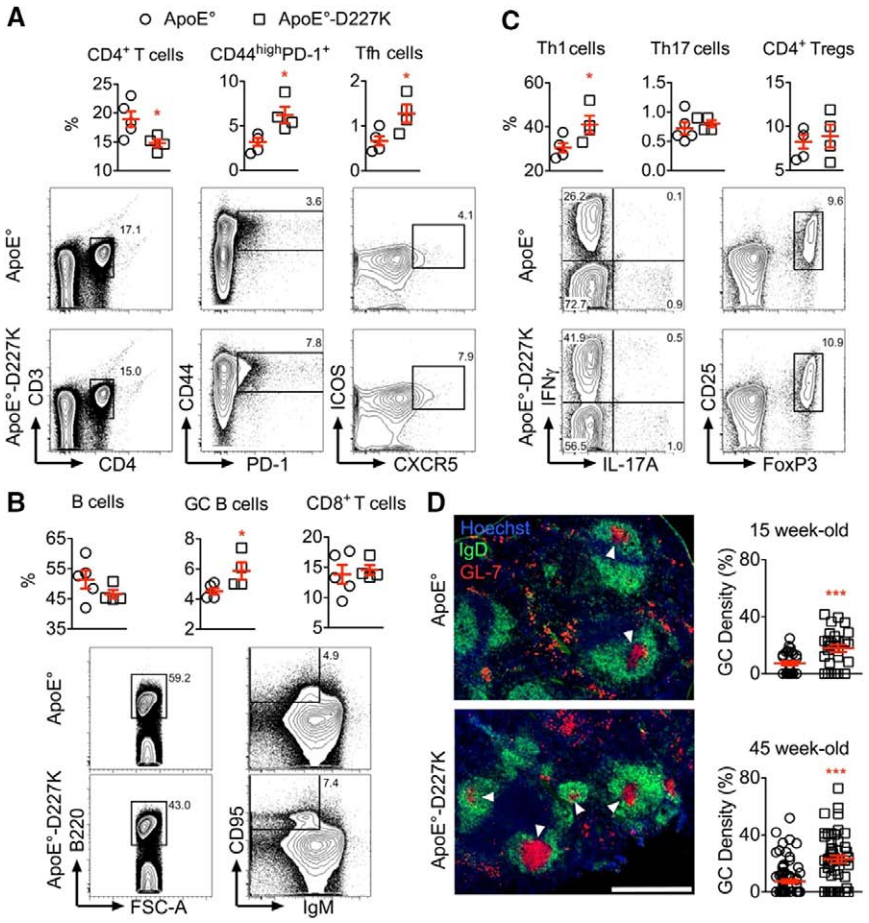

Figure 2. Genetic invalidation of CD8⁺ regulatory T cell (Treg) function exacerbates atherosclerosis. Flow cytometry analysis of (**A**) total CD4⁺ T cells (among CD45⁺ cells), CD44^{high}PD-1⁺ activated memory (among CD45⁺ cells) T cells, T follicular helper (Tfh) cells (among CD45⁺ cells), (**B**) total B220⁺ B cells (among CD45⁺ cells), CD95^{high}IgM^{low} germinal center (GC) B cells (among CD45⁺ cells), CD8⁺ T cells (among CD45⁺ cells), and (**C**) Th1 (interferon [IFN]-γ⁺), Th17 (interleukin [IL]-17A⁺), and CD25^{high}FoxP3⁺CD4⁺ Treg cells (among CD4⁺ cells) performed on splenocytes from 35-week-old apolipoprotein E–knockout (ApoE°; n=5) and ApoE°-D227K (n=4) mice. **D**, Immunofluorescence staining on spleen cryosections from 15-week-old ApoE° and ApoE°-D227K mice stained for IgD, GL-7, and nuclei (Hoechst). Arrowheads indicate the GCs (GL-7⁺) within the B-cell follicles. The graphs on the **right** represent the quantification of the GC density in 15- and 45-week-old ApoE° and ApoE°-D227K mice (scale bar, 500 μm). *P<0.05, ***P<0.001, Mann–Whitney test (**A**–**C**) and Student t test (**D**).

of total B cells and CD8⁺ T cells were equivalent to those in ApoE° mice (Figure 2B). The GL-7/IgD surface-to-area ratio was also significantly increased in the ApoE°-D227K mice (Figure 2D), indicating greater Ig class-switching activity in their splenic B-cell follicles compared with the age-matched ApoE° mice. This finding was corroborated by an increased plasma cell population in the spleen (but not lymph nodes) of aged ApoE°-D227K mice (Figure IID in the online-only Data Supplement).

In contrast, the peritoneal B-1 cell populations were not affected by the D227K mutation (Figure IIE in the online-only Data Supplement). Of note, CD4⁺ Th1 polarization was augmented in the ApoE°-D227K mice compared with the ApoE° mice (Figure 2C). Additionally, the 2 groups of mice had similar proportions of Th17 cells and CD25⁺FoxP3⁺ CD4⁺ Tregs.

These results indicate that the impaired function of CD8⁺ Tregs in ApoE°-D227K mice leads to a specific strengthening of the Tfh-GC B-cell axis and rules out the involvement of the CD4⁺ Treg population.

Defective Tfh Cell Regulation by CD8⁺ Tregs Accelerates Atherogenesis

The previous experiments collectively indicated that the control of Tfh cells by CD8⁺ Tregs limits lesion development in ApoE° mice. To conclusively address this issue, we transferred CD4⁺ T cells that were sensitive (from ApoE° mice) or insensitive (from ApoE°-D227K mice) to control by CD8⁺ Tregs into ApoE° mouse recipients (Figure 3A). ApoE° and ApoE°-D227K cell preparations had equivalent cell compositions (Figure IIIA in the online-only Data Supplement).

Twenty weeks after the first injection, atherogenesis was accelerated in the ApoE° mice that received the CD4⁺ T cells from the ApoE°-D227K mice (ApoE°-D227K→ApoE°; n=10; Figure 3A). The proportions of splenic CD4⁺ T cells, activated memory cells, and Tfh cells were also increased compared with the proportions in the ApoE°→ApoE° recipient mice (n=9; Figure 3B). There were no differences between the 2 groups with respect to the frequencies of the splenic Th1, Th17, and Th2 populations (Figure 3C). Importantly, the percentage of splenic GC B cells increased in the ApoE°-D227K→ApoE° mice compared with the ApoE°→ApoE° mice (Figure 3D). Accordingly, the number of B cell follicles (IgD⁺) and the number and density of GCs (IgD⁻GL-7⁺) were also increased, whereas the size of the B-cell follicles did not change (Figure 3E), indicating a specific effect on the GC reaction. In addition, the plaques of the ApoE°-D227K→ApoE° mice displayed a nonstable phenotype, with enhanced deposits of IgG (but not IgM), increased infiltration of CD68⁺ macrophages, and decreased α-smooth muscle actin content (Figure 3F and Figure IIIB in the online-only Data Supplement).

Restoring Tfh Control in ApoE°-D227K Mice Reduces Atherosclerosis

To restore the control of the expanded Tfh cells observed in the ApoE°-D227K mice or to reduce, if possible, the limited

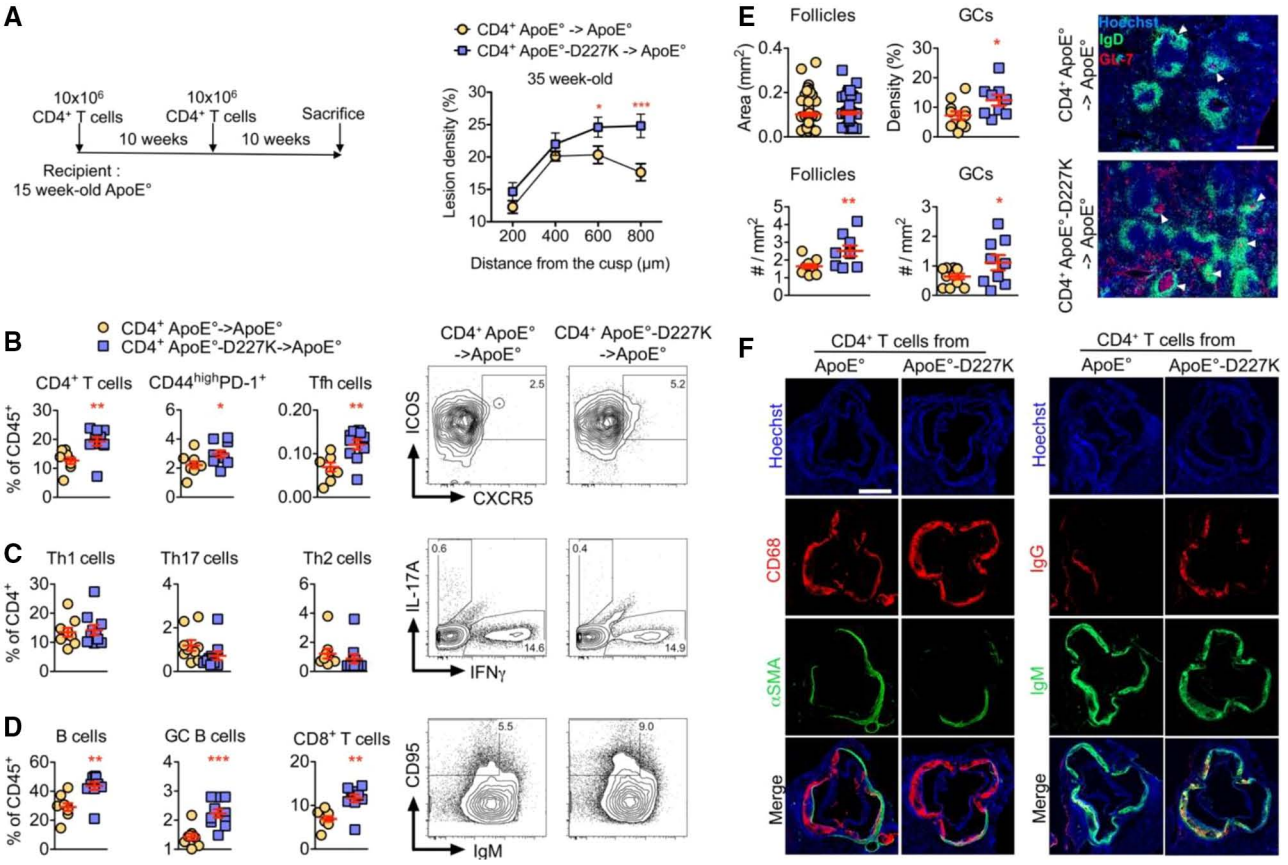

Figure 3. CD8⁺ regulatory T cells (Tregs) control atherosclerosis, at least in part, by blocking T follicular helper (Tfh) expansion in apolipoprotein E–knockout (ApoE°) mice. ApoE° mice (n=9–10 per group) were infused twice intravenously with 10×10^6 total splenic CD4⁺ cells (at 15 and 25 weeks of age) from 8-week-old ApoE° or ApoE°-D227K mice. **A**, Atherosclerotic lesions in the aortic root measured 20 weeks after the first injection. **B**, Total CD4⁺ T cells, CD44^{high}PD-1⁺ activated memory T cells, and Tfh cells (among CD45⁺ cells); (**C**) interferon-γ⁺ Th1, interleukin [IL]-17A⁺ Th17, and IL-4⁺ Th2 cells (among CD4⁺ cells); and (**D**) total B220⁺ B cells, CD95^{high}IgM^{low} germinal center (GC) B cells, and CD8⁺ T cells (among CD45⁺ cells) analyzed by flow cytometry in spleens from ApoE° mice infused with CD4⁺ T cells from ApoE° (CD4⁺ ApoE°→ApoE°) and ApoE°-D227K mice (CD4⁺ApoE°-D227K→ApoE°). **E**, Quantitative analysis of the number and area of B-cell follicles and GCs in the spleens of CD4⁺ApoE°→ApoE° and CD4⁺ApoE°-D227K→ApoE° mice. **Right**, Immunostaining of spleen cryosections from CD4⁺ApoE°→ApoE° and CD4⁺ApoE°-D227K→ApoE° mice stained for IgD, GL-7, and nuclei (Hoechst). Arrowheads indicate the GCs (GL-7⁺) within the B-cell follicles (scale bar, 500 µm). **F**, Immunofluorescent staining of aortic root cryosections from CD4⁺ApoE°→ApoE° and CD4⁺ApoE°-D227K→ApoE° mice stained for CD68 and α-smooth muscle actin (αSMA) or IgG, IgM, and nuclei (Hoechst; scale bar, 500 µm). *P<0.05, **P<0.01, ***P<0.001, 2-way ANOVA (**A**), Mann–Whitney test (**B**–**D**), and Student t test (**E**).

contingent of Tfh cells in the ApoE° mice, mice from both genotypes were treated with an anti-ICOSL antibody (known to impair Tfh cell development)[19,20] or an isotype control for 10 weeks (n=9–10 per group). Strikingly, the anti-ICOSL treatment normalized atherosclerosis development in the ApoE°-D227K mice (but not in ApoE° mice) to the level in the isotype control–treated ApoE° mice (Figure 4A). Additionally, the intraplaque IgG deposits were drastically reduced in the anti-ICOSL–treated ApoE°-D227K mice (Figure 4B and Figure IVA in the online-only Data Supplement). IgG was also decreased, although to a lower extent, in the treated ApoE° mice, in which there was also a decrease in the CD68⁺ macrophage intraplaque content (Figure 4C and Figure IVA in the online-only Data Supplement).

The anti-ICOSL treatment significantly reduced the percentages of splenic Tfh and activated memory cells (but not of total CD4⁺ T cells) in ApoE°-D227K mice (Figure 4D and Figure IVB in the online-only Data Supplement) and had no effect on Th1 cells, Th17 cells, or CD4⁺ Tregs (Figure 4E). Furthermore, the administration of the anti-ICOSL antibody did not modify the percentage of CD8⁺ T cells or B cells but significantly inhibited the expansion of GC B cells in the spleen of the ApoE°-D227K mice and, to a lesser extent, of the ApoE° mice (Figure 4F and Figure IVB and IVC in the online-only Data Supplement).

These results show that the impact of the anti-ICOSL antibody treatment was maximal in the ApoE°-D227K mice, in which it significantly reduced the size of the Tfh cell compartment, limited the GC reaction, and drastically reduced lesion development.

Tfh Cells Regulate the Formation and Maintenance of Aortic TLOs

We found that CD23 was expressed by most of the CD19⁺ B cells in the aortas of 45-week-old ApoE° mice (n=5; 2 experiments) and that only 10% of the B cells expressed the CD5 B-1a cell marker (Figure VA in the online-only Data Supplement). Analysis of the CD5⁺ B-cell population

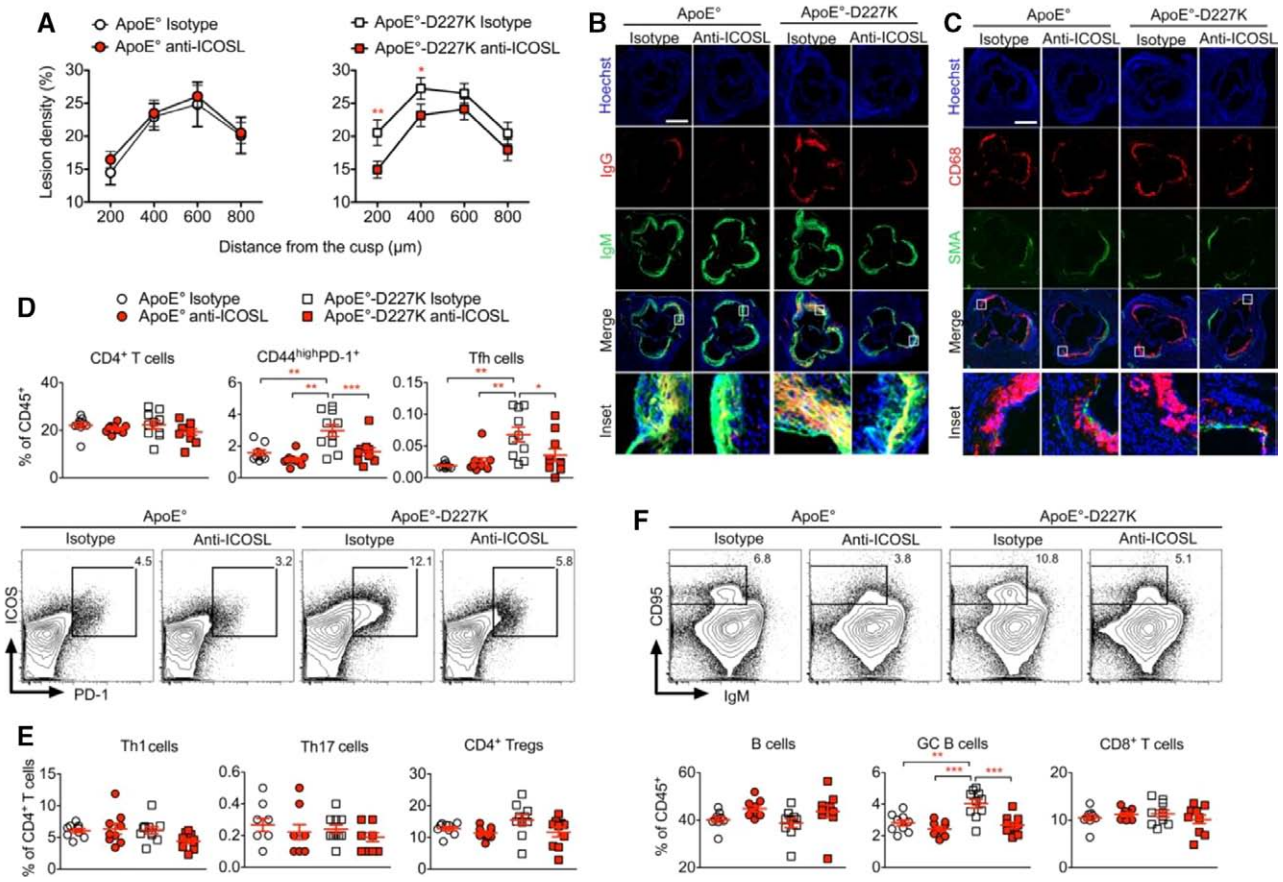

Figure 4. Blocking ICOSL signaling rescues T follicular helper (Tfh) regulation in apolipoprotein E–knockout (ApoE°)-D227K mice. Fifteen-week-old ApoE° and ApoE°-D227K female mice were injected intraperitoneally for 10 weeks with an anti-ICOSL antibody or isotype control (100 μg/wk; n=9–10 mice per group). **A**, Size of the aortic root atherosclerotic lesions in antibody-treated ApoE° and ApoE°-D227K mice. Immunofluorescent staining of aortic root cryosections from ApoE° and ApoE°-D227K±anti-ICOSL/isotype control mice that were stained for (**B**) IgD and IgM or (**C**) CD68 and α-smooth muscle actin (αSMA) and nuclei (Hoechst). The square boxes represent the areas magnified below (scale bar, 500 μm). **D**, Total $CD4^+$ T cells, $CD44^{high}PD\text{-}1^+$ activated memory T cells, and Tfh cells (among $CD45^+$ cells); (**E**) interferon-γ^+ Th1, interleukin-$17A^+$ Th17, and $CD25^{high}FoxP3^+CD4^+$ regulatory T cell (Treg) cells (among $CD4^+$ cells); and (**F**) $B220^+$ B cells, $CD95^{high}IgM^{low}$ germinal center (GC) B cells, and $CD8^+$ T cells (among $CD45^+$ cells) analyzed by flow cytometry in spleens from antibody-treated ApoE° and ApoE°-D227K mice. *P<0.05, **P<0.01, ***P<0.001, 2-way ANOVA with the Tukey post hoc test (**A** and **D**–**F**).

for the expression of CD11b (high), B220 (low), and IgM confirmed the B-1 phenotype of these cells. In total, 1% of the B cells within the adventitia were GC B cells ($CD95^{high}$; Figure VB in the online-only Data Supplement). Analysis of the $CD45^+$ leukocytes in the aortas of the ApoE° and ApoE°-D227K mice revealed that the percentages of B and $CD4^+$ T cells did not differ between the 2 mouse models. However, the proportions of activated memory and Tfh cells were significantly increased in the aortas of the ApoE°-D227K mice (n=8) compared with ApoE° mice (n=9; Figure 5A and 5B). The topographical distribution of B cells in the aortas was then analyzed in ApoE° and ApoE°-D227K mice on whole-mount preparations of the adventitial layer labeled with a B220 B-cell–specific antibody.[10] B cells were clustered into TLO structures identified as $B220^+$ B-cell follicles supplied with isolectin $B4^+$ blood vessels and drained by $Gp38^+$ lymphatic vessels (Figure 5C). Interestingly, the ApoE°-D227K mice (n=52) developed a greater number of adventitial B-cell clusters, which appeared earlier than in the ApoE° (n=49) and ApoE°–Qa-1° (n=27) mice (Figure 5D). Finally, anti-ICOSL antibody treatment reduced the number of B cell clusters in the adventitias of the ApoE° and ApoE°-D227K mice (Figure 5E).

This set of data strongly suggests that Tfh cells are involved in the formation or maintenance of adventitial TLOs.

TLOs in Human Atherosclerotic Aneurysmal Arteries

The observations made in our mouse model are relevant to human atherothrombosis because in most of the clinical samples of atherosclerotic AAAs that we collected, we detected mature TLOs, which can be coarsely identified by hematoxylin and eosin staining (Figure 6A). Additionally, $CD20^+$ B-cell follicles surrounded by $PNAd^+$ high endothelial venules were observed (Figure 6B). The B-cell follicles were structurally similar to the ones described in secondary lymphoid organs, and most of them contained GCs, as characterized by the presence of $Gp38^+CD21^+$ follicular dendritic cells (Figure 6C). The expression of homeostatic chemokines such as CXCL13 by follicular dendritic, Tfh, and B cells likely participates in the maintenance of the compartmentalized organization of these structures (Figure 6B and 6C).[21] Importantly, although

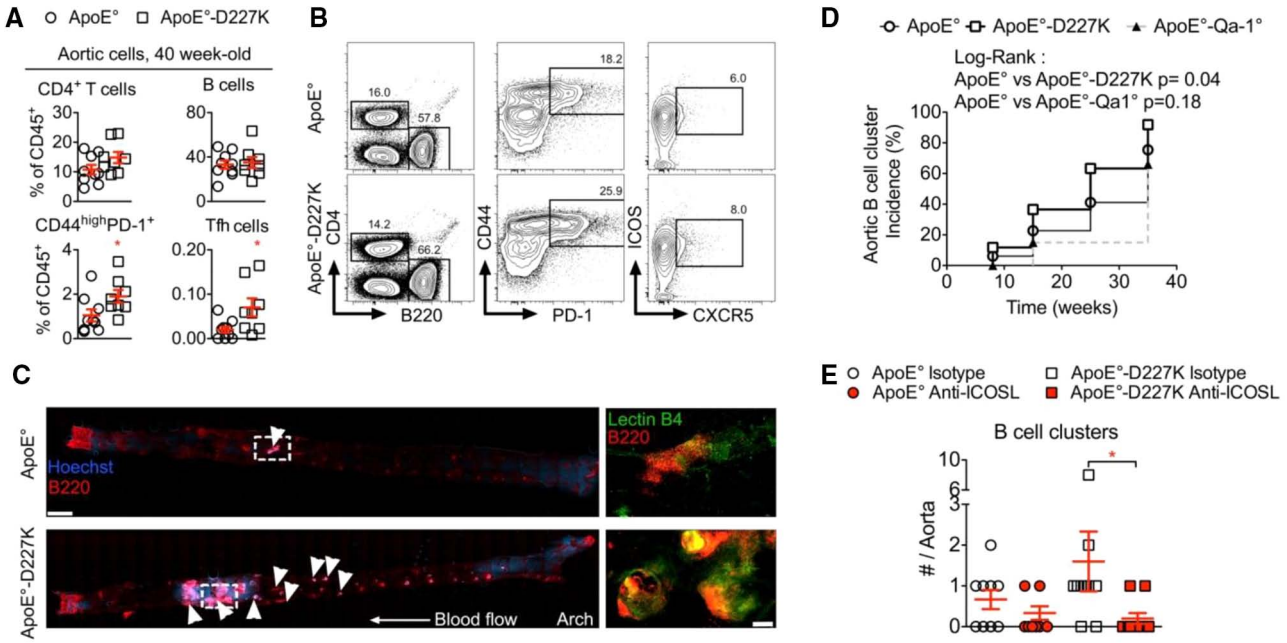

Figure 5. T follicular helper (Tfh) cell function is required for the induction and maintenance of tertiary lymphoid organs in apolipoprotein E–knockout (ApoE°) mice. **A** and **B**, Flow cytometry analysis of total CD4+ T cells, CD44highPD-1+ activated memory T cells, B220+ B cells, and Tfh cells (among live CD45+ cells) performed on digested aortas from 40-week-old ApoE° (n=9) and ApoE°-D227K mice (n=8). **C**, Whole mounts of the entire aortic adventitia from 35-week-old ApoE° and ApoE°-D227K mice stained for B220 (B cells), isolectin B4 (vessels), and nuclei (Hoechst). Arrowheads indicate the B220+ B-cell clusters along the aorta. The dashed square boxes point to the areas magnified on the **right** (scale bar, 2 mm). **D**, Incidence of aortic B-cell clusters in the aortas of ApoE° (n=49), ApoE°-D227K (n=52), and ApoE°–Qa-1° mice (n=27). **E**, B-cell cluster number in the aortas of ApoE° and ApoE°-D227K mice injected with anti-ICOSL or isotype control antibodies. **P*<0.05, Mann–Whitney test (**A**), log-rank test (**D**), and 2-way ANOVA with the Tukey post hoc test (**E**).

only nonorganized lymphoid aggregates were detected in early atherosclerotic lesions, we found TLOs similar to those of AAAs in the few nonaneurysmal aortas with advanced atherosclerotic lesions that were studied (Figure VI in the online-only Data Supplement).

A paired comparison of the leukocytes within the blood and adventitia of the same patient revealed a dramatic enrichment (5-fold) of B cells within the adventitia (Figure 6D). This finding indicated that B cells that infiltrate into atherothrombotic aneurysmal aortas are not a mere representation of systemic patrolling B cells but rather are B cells that are specifically attracted to or locally generated in the adventitia. Indeed, the phenotypes of the B cells in the 2 compartments were not the same, with an increase in memory B cells ($IgD^-CD38^-CD27^{high}$), GC B cells (IgD^-CD38^+), and plasma cells (IgD^-CD38^{high}), together with a decreased proportion of naïve B cells ($IgD^+CD38^-CD27^{low}$), within the adventitia compared with the paired blood sample (the decrease in CD27 brightness in the adventitia resulted from the digestion process; Figure 6D). Absolute quantification of the cells within the adventitias of AAAs revealed an increase in $CD45^+$ cells compared with cells in the nonaneurysmal adventitia (N-AA) samples (Figure 6E). The adventitias of the AAAs (n=8) also showed a strong increase in the number of $HLA\text{-}DR^+CD19^+$ cells and in various adventitial B-cell subsets compared with the N-AA adventitias (n=13; Figure 6E). Pre-GC B cells, GC cells, and plasma cells, which were virtually absent from the adventitias of the N-AAs, could also be detected in the adventitias of the aneurysms (Figure 6E).

The Adventitia of Aneurysmal Aortas Releases Immunoglobulins and Tfh-Related Cytokines

We next examined the release of immunoglobulins and cytokines from conditioned medium (CM) prepared from the adventitial layers of N-AAs (n=15) and AAAs (n=15) to document the functionality of the adventitial TLOs. All classes of immunoglobulins were increased in the CM from the AAAs compared with the N-AAs (Figure 7A). We found that cytokines known to participate in T-cell survival (interleukin [IL]-2, IL-7), T-cell effector function (interferon-γ, IL-17A, IL-4), inflammation (IL-1β, tumor necrosis factor-α), and B-cell function (IL-21, CD40L, IL-10) were increased in the CM from the AAAs compared with the control aortas (Figure 7B). Among the tested cytokines, IL-21 is particularly relevant to the immunobiology of TLOs because it is produced predominantly by Tfh cells and is essential for B-cell activation, B-cell expansion, and plasma cell generation.[22] Remarkably, we found significant positive correlations between the amount of IL-21 and the amounts of IgG1, IgG4, and total immunoglobulins within the CM. Strikingly, the concentration of IL-21 in the CM from the AAAs positively correlated with the AAA diameter (Figure 7C).

Collectively, these data demonstrate that Tfh cells are present in the adventitias of human AAAs, where they may participate in the progression of the disease by promoting the local maturation of seemingly pathogenic B cells. Therefore, we next assessed whether we could directly detect and isolate Tfh cells from human aortas by flow cytometry.

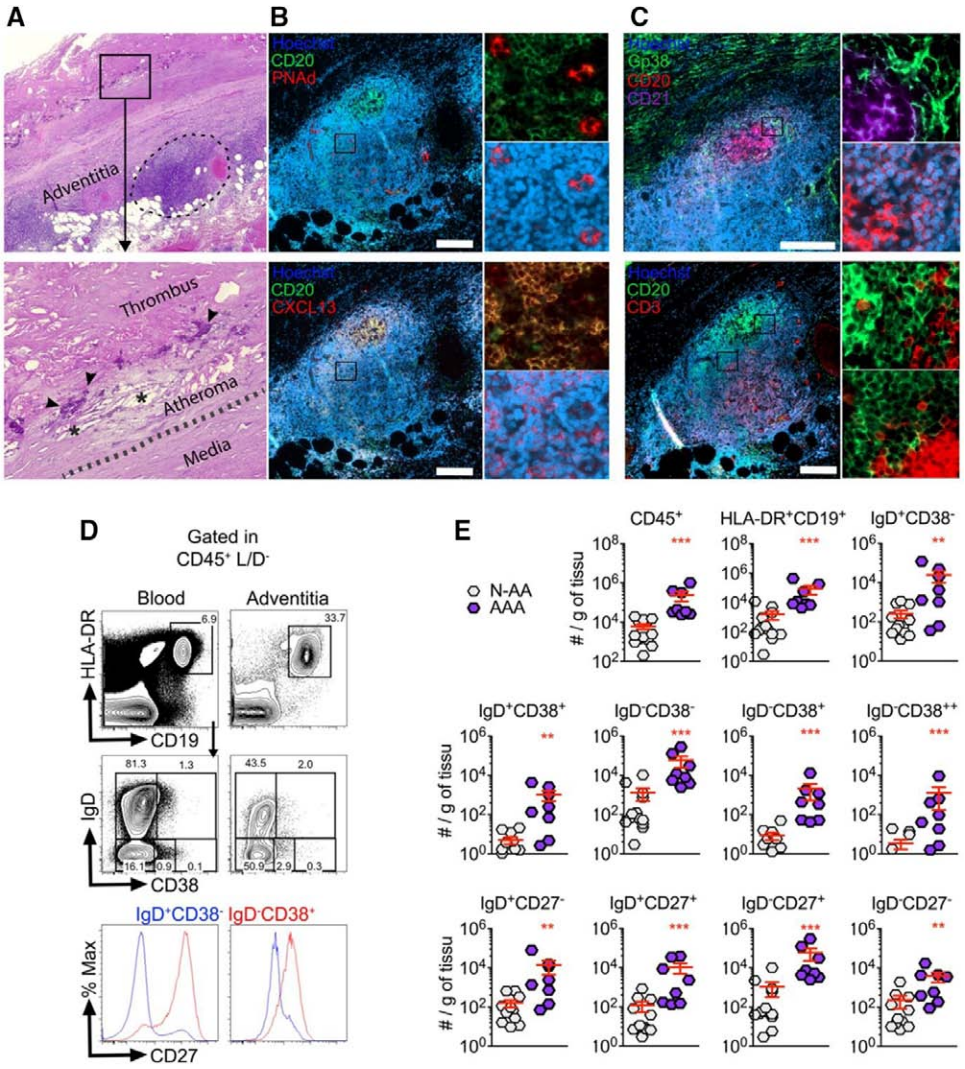

Figure 6. B-cell follicles develop in the adventitias of human abdominal aortic aneurysms (AAAs). **A**, Hematoxylin-eosin staining of human AAA cryosections; the adventitial position of a tertiary lymphoid organ is indicated by the dashed line. Inset, A magnification of the luminal layers comprising an atherosclerotic lesion beneath the mural thrombus that is identified by the presence of cholesterol clefts (asterisks) and calcifications (arrowheads). Serial cryosections stained for (**B**) CD20, PNAd, CXCL13, and nuclei (Hoechst) or (**C**) Gp38, CD20, CD21, CD3, and nuclei (Hoechst). The framed areas are magnified on the **right** (scale bar, 200 μm). **D**, Total HLA-DR$^+$CD19$^+$ B cells (among L/D$^-$ live CD45$^+$ cells), IgD$^+$CD38$^-$CD27^{low} naïve, IgD$^-$CD38$^-$CD27^{high} memory, IgD$^-$CD38$^+$ germinal center (GC) B cells, and IgD$^-$CD38^{++} plasma cells (among HLA-DR$^+$CD19$^+$ cells) compared between human blood and adventitial digests from the same AAA patient. **E**, Absolute quantification of several B-cell subsets in adventitial digests from AAA and nonaneurysmal (N-AA) tissues (n=8 and 13 per group, respectively). $^{**}P<0.01$, $^{***}P<0.001$, Mann–Whitney test (**E**).

Tfh Cells Are Present in the Adventitias of Human AAAs

Analysis of the CD45$^+$ cells in the adventitias of the AAAs (n=8) revealed a high percentage of CD4$^+$ T cells compared with the percentage in the N-AAs (n=14). These T-helper cells were mostly CD45RO$^+$, and in the adventitias from AAAs, some expressed canonical Tfh cell markers such as CXCR5, ICOS, and PD-1 (Figure 8A). Compared with the N-AAs, the adventitias of the AAAs displayed a significant increase in CD45RO$^-$ naïve and CD45RO$^+$ memory CD4$^+$ T cells and a slight increase in CD8$^+$ T cells (Figure 8B). Immunohistological analysis of the AAA adventitias (n=5) confirmed the presence of CD3$^+$CXCR5$^+$ Tfh cells in the B-cell follicles of TLOs undergoing GC reactions (presence of follicular dendritic cells and AICDA$^+$ B cells), as depicted in Figure 8C.

To further characterize these Tfh cells, they were sorted by fluorescence-activated cell sorter analysis (n=9 AAAs; Figure VIIA in the online-only Data Supplement), and their gene expression was analyzed by real-time quantitative polymerase chain reaction (Figure VIIB in the online-only Data Supplement). Our data confirmed that the adventitial Tfh cells had a specific transcriptomic profile that distinguished them from CD4$^+$ naïve cells, memory cells, and Tregs (Figure 8D). The naïve CD4$^+$ T cells were characterized by their strong expression of CCR7, and the memory CD4$^+$ T cells expressed Th1/17-associated genes (TBX21, interferon-γ, IL-17A). Additionally, the CD4$^+$ Tregs expressed CTLA4, FoxP3, GATA3, c-MAF, and SH2D1A. The sorted Tfh cells strongly expressed IL-21, CXCL13, c-MAF, BATF, OX40, BTLA, and SH2D1A, that is, molecules required for B-cell

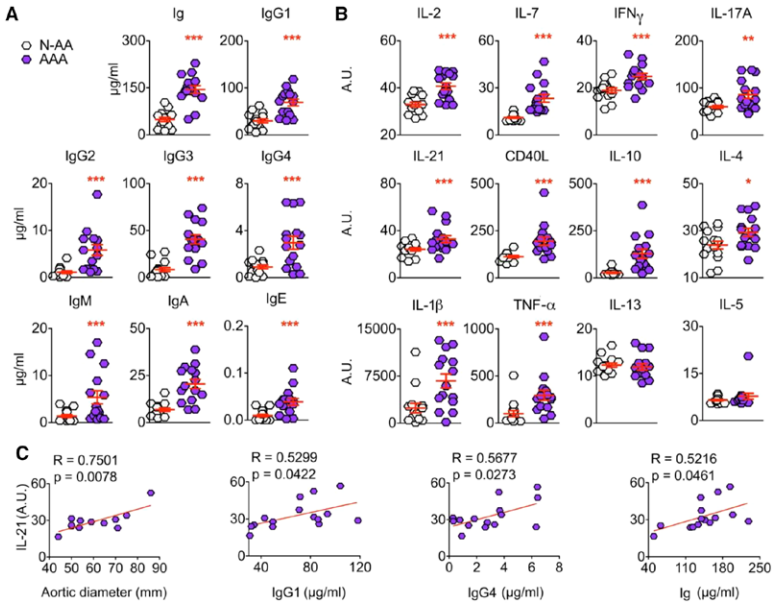

Figure 7. Adventitias from human abdominal aortic aneurysms (AAAs) release immunoglobulins and T follicular helper (Tfh)–associated proteins. Quantification of (**A**) immunoglobulin (total Ig, IgG1, IgG2, IgG3, IgG4, IgM, IgA, and IgE; µg/mL) and (**B**) cytokine (interleukin [IL]-2, IL-7, interferon [IFN]-γ, IL-17A, IL-21, CD40L, IL-10, IL-4, IL-1β, tumor necrosis factor [TNF]-α, IL-13, and IL-5; arbitrary units [A.U.]) concentrations assessed on conditioned medium (CM) from AAA and nonaneurysmal tissues (n=15 per group). **C**, Correlation plots between IL-21 concentration (AU) and aorta diameter, IgG1, IgG4, and total Ig concentrations in the CM from the AAA tissues. **P*<0.05, ***P*<0.01, ****P*<0.001, Student *t* test (**A** and **B**).

function (Figure 8D and Figure VIIB in the online-only Data Supplement). Notably, genome-wide association studies revealed that *MAF* and *CXCL13* gene polymorphisms are associated with cardiovascular diseases/risk factors.[23] In addition, the extensive transcriptomic study performed by Lenk et al[24] revealed that most of the genes (except *BCL6*) involved in Tfh cell biology are upregulated in noninflammatory human AAAs compared with control aortas.

Therefore, the adventitias of human AAAs are infiltrated by Tfh cells that display some canonical features of secondary lymphoid organ Tfh cells, in particular those involved in the help that Tfh cells provide to B cells. Accordingly, the

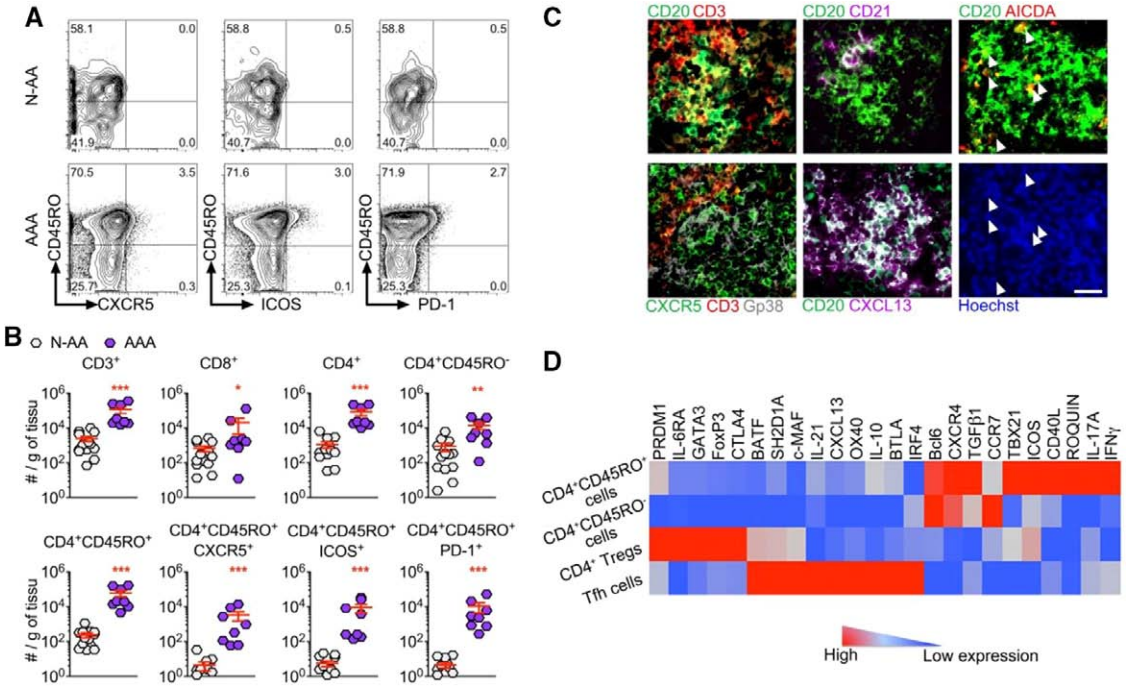

Figure 8. Characterization of T follicular helper (Tfh) cells in the adventitias of human abdominal aortic aneurysms (AAAs). **A**, Flow cytometry analysis of the expression of CD45RO, CXCR5, ICOS, and PD-1 on CD4⁺ T cells in aortic digests from AAA and nonaneurysmal (N-AA) tissues. **B**, The absolute number (per 1 g tissue) of total CD3⁺, CD8⁺, CD4⁺, CD4⁺CD45RO⁻, CD4⁺CD45RO⁺, CD4⁺CD45RO⁺CXCR5⁺, CD4⁺CD45RO⁺ICOS⁺, and CD4⁺CD45RO⁺PD-1⁺ T cells analyzed by flow cytometry in aortic digests from AAA and N-AA tissues (n=8 and 14 per group, respectively). **C**, Immunofluorescence analysis of human tertiary lymphoid organs in AAA cryosections stained for CD20, CD3, CXCR5, gp38, CD21, CXCL13, AICDA, and nuclei (Hoechst). Arrowheads point at switched B cells (positive for CD20 and AICDA; scale bar, 25 µm). **D**, RNA expression of T cell–related genes analyzed in purified, cell-sorted CD45RO⁻ naïve, CD45RO⁺ memory, and CD25^{high}CD127^{low} regulatory CD4⁺ T cells (Tregs) and in Tfh cells in aortic digests from human AAAs (n=9). IFN-α indicates interferon-α; and IL, interleukin. **P*<0.05, ***P*<0.01, ****P*<0.001, Mann–Whitney test (**B**).

Tfh cells were found nearly exclusively within the adventitial B-cell follicles.

Discussion

Intensive investigations in the fields of atherosclerosis and vascular biology have identified the regulatory mechanisms that govern the immune response involved in plaque growth.[25–28] Initial studies[1,29,30] indicated the atheroprotective potential of the B-cell compartment that relies on B1a cells and germ-line–encoded immunoglobulins. In contrast, recent studies have identified T-dependent B cells (B2 cells) as potent proatherogenic mediators in the ApoE° and low-density lipoprotein receptor–knockout mouse models.[3,4] B-cell activation, proliferation, and function are orchestrated by Tfh cells,[11] the regulation of which is crucial to avoid the development of self-reactive humoral responses.[31] This regulation can be performed by Qa-1–restricted CD8$^+$ Tregs.[14] Our data now demonstrate that through their control of Tfh cell function, CD8$^+$ Tregs are potent modulators of atherogenesis.

We first found a concomitant expansion of Tfh and GC B cells in parallel with a loss of CD8$^+$ Tregs during atherosclerosis development in ApoE° mice. The further impaired function of CD8$^+$ Tregs triggered in the ApoE°-D227K mice led to overactivation of the Tfh-GC B-cell axis. Remarkably, this event favored the development of atherosclerosis. Restoring control of the Tfh-GC B cell axis by blocking the ICOS-ICOSL interaction reduced lesion development in the ApoE°-D227K mice. In addition, for the first time, we describe the involvement of Tfh cells in the formation and maintenance of adventitial ectopic GCs in atherothrombotic arteries. Finally, we show that these observations are fully relevant to human disease because we could comprehensively characterize Tfh cells in human atherothrombotic aortas.

TLOs cannot be considered passive bystander markers of tissue inflammation because their formation marks a turning point in chronic inflammatory processes. In alloimmune responses, TLOs promote the antibody-mediated destruction of grafts.[32–34] In autoimmune diseases, TLOs are clearly detrimental, promoting autoantibody production and activating cellular effectors, both of which result in organ damage.[34,35] In the present study, we report that atherosclerosis development in ApoE° mice is characterized by an expansion of Tfh cells within aortic adventitial TLOs and that TLO development and maintenance are dependent on the Tfh cell compartment. Although we could not correlate TLO formation with plaque development (our whole-mount technique requires the separation of the adventitia from the rest of the vessel), it is important to note that Gräbner et al[9] have demonstrated that TLO size is correlated with plaque size and that TLOs always develop in atherosclerotic arterial segments in ApoE° mice.

We also fully characterized the presence and functional phenotype of Tfh cells in the adventitial TLOs of human AAA. The adventitial tissue of AAAs released immunoglobulins, thereby indicating that adventitial TLOs are functional B-cell structures. Strikingly, in the CM of AAA adventitia, the concentration of IL-21, a prototypic Tfh cell cytokine, was positively correlated with the diameter of the aneurysm, strongly suggesting that the Tfh-dependent B-cell response is directly linked to the progression of the disease. In addition to IL-21, the adventitial layer of AAAs is an inflamed microenvironment where high concentrations of many cytokines are detected. We believe that the topological organization of the arterial wall places the adventitia in a position where it concentrates most of the soluble/particulate mediators that percolate radially from the lesions,[36] thereby resulting in a high inflammatory profile that promotes lymphoid neogenesis on this layer.

Conclusions

We found that the Tfh-GC B-cell axis is centrally involved in the development of mouse and human atherosclerosis. We show that this axis is under the control of CD8$^+$ Tregs and provide the first line of evidence indicating that, beyond their role in secondary lymphoid organs, Tfh cells are also key players in the GC reaction that develops in TLOs (Figure VIII in the online-only Data Supplement). This study therefore paves the way for innovative therapeutic strategies targeting this axis.

Sources of Funding

This work was supported by the Institut National de la Santé et de la Recherche Médicale (INSERM), Paris Denis Diderot University, the Région Ile de France, the Fondation de la Recherche Médicale, the Fondation de France, and the Agence Nationale de la Recherche (grant MI2 ATHLO).

Disclosures

None.

References

1. Nicoletti A, Kaveri S, Caligiuri G, Bariéty J, Hansson GK. Immunoglobulin treatment reduces atherosclerosis in apo E knockout mice. *J Clin Invest*. 1998;102:910–918. doi: 10.1172/JCI119892.
2. Kyaw T, Tay C, Krishnamurthi S, Kanellakis P, Agrotis A, Tipping P, Bobik A, Toh BH. B1a B lymphocytes are atheroprotective by secreting natural IgM that increases IgM deposits and reduces necrotic cores in atherosclerotic lesions. *Circ Res*. 2011;109:830–840. doi: 10.1161/CIRCRESAHA.111.248542.
3. Kyaw T, Tay C, Khan A, Dumouchel V, Cao A, To K, Kehry M, Dunn R, Agrotis A, Tipping P, Bobik A, Toh BH. Conventional B2 B cell depletion ameliorates whereas its adoptive transfer aggravates atherosclerosis. *J Immunol*. 2010;185:4410–4419. doi: 10.4049/jimmunol.1000033.
4. Ait-Oufella H, Herbin O, Bouaziz JD, Binder CJ, Uyttenhove C, Laurans L, Taleb S, Van Vré E, Esposito B, Vilar J, Sirvent J, Van Snick J, Tedgui A, Tedder TF, Mallat Z. B cell depletion reduces the development of atherosclerosis in mice. *J Exp Med*. 2010;207:1579–1587. doi: 10.1084/jem.20100155.
5. Aloisi F, Pujol-Borrell R. Lymphoid neogenesis in chronic inflammatory diseases. *Nat Rev Immunol*. 2006;6:205–217. doi: 10.1038/nri1786.
6. Dutertre CA, Clement M, Morvan M, Schäkel K, Castier Y, Alsac JM, Michel JB, Nicoletti A. Deciphering the stromal and hematopoietic cell network of the adventitia from non-aneurysmal and aneurysmal human aorta. *PLoS One*. 2014;9:e89983. doi: 10.1371/journal.pone.0089983.
7. Saphir O, Gore I. Evidence for an inflammatory basis of coronary arteriosclerosis in the young. *Arch Pathol* 1950;49:418–426.
8. Houtkamp MA, de Boer OJ, van der Loos CM, van der Wal AC, Becker AE. Adventitial infiltrates associated with advanced atherosclerotic plaques: structural organization suggests generation of local humoral immune responses. *J Pathol*. 2001;193:263–269. doi: 10.1002/1096-9896(2000)9999:9999<::AID-PATH774>3.0.CO;2-N.
9. Gräbner R, Lötzer K, Döpping S, Hildner M, Radke D, Beer M, Spanbroek R, Lippert B, Reardon CA, Getz GS, Fu YX, Hehlgans T, Mebius RE, van der Wall M, Kruspe D, Englert C, Lovas A, Hu D, Randolph GJ, Weih F, Habenicht AJ. Lymphotoxin beta receptor signaling promotes tertiary lymphoid organogenesis in the aorta adventitia of aged ApoE-/- mice. *J Exp Med*. 2009;206:233–248. doi: 10.1084/jem.20080752.
10. Guedj K, Khallou-Laschet J, Clement M, Morvan M, Gaston AT, Fornasa G, Dai J, Gervais-Taurel M, Eberl G, Michel JB, Caligiuri G, Nicoletti

A. M1 macrophages act as LTβR-independent lymphoid tissue inducer cells during atherosclerosis-related lymphoid neogenesis. *Cardiovasc Res*. 2014;101:434–443.
11. Tangye SG, Ma CS, Brink R, Deenick EK. The good, the bad and the ugly: TFH cells in human health and disease. *Nat Rev Immunol*. 2013;13:412–426. doi: 10.1038/nri3447.
12. Varthaman A, Clement M, Khallou-Laschet J, Fornasa G, Gaston AT, Dussiot M, Caligiuri G, Cantor H, Kaveri S, Nicoletti A. Physiological induction of regulatory Qa-1-restricted CD8+ T cells triggered by endogenous CD4+ T cell responses. *PLoS One*. 2011;6:e21628. doi: 10.1371/journal.pone.0021628.
13. Varthaman A, Khallou-Laschet J, Clement M, Fornasa G, Kim HJ, Gaston AT, Dussiot M, Caligiuri G, Herbelin A, Kaveri S, Cantor H, Nicoletti A. Control of T cell reactivation by regulatory Qa-1-restricted CD8+ T cells. *J Immunol*. 2010;184:6585–6591. doi: 10.4049/jimmunol.0903109.
14. Kim HJ, Verbinnen B, Tang X, Lu L, Cantor H. Inhibition of follicular T-helper cells by CD8(+) regulatory T cells is essential for self tolerance. *Nature*. 2010;467:328–332. doi: 10.1038/nature09370.
15. Kim HJ, Wang X, Radfar S, Sproule TJ, Roopenian DC, Cantor H. CD8+ T regulatory cells express the Ly49 Class I MHC receptor and are defective in autoimmune prone B6-Yaa mice. *Proc Natl Acad Sci USA*. 2011;108:2010–2015. doi: 10.1073/pnas.1018974108.
16. Jiang H, Canfield SM, Gallagher MP, Jiang HH, Jiang Y, Zheng Z, Chess L. HLA-E-restricted regulatory CD8(+) T cells are involved in development and control of human autoimmune type 1 diabetes. *J Clin Invest*. 2010;120:3641–3650. doi: 10.1172/JCI43522.
17. Lu L, Kim HJ, Werneck MB, Cantor H. Regulation of CD8+ regulatory T cells: Interruption of the NKG2A-Qa-1 interaction allows robust suppressive activity and resolution of autoimmune disease. *Proc Natl Acad Sci USA*. 2008;105:19420–19425. doi: 10.1073/pnas.0810383105.
18. Hu D, Ikizawa K, Lu L, Sanchirico ME, Shinohara ML, Cantor H. Analysis of regulatory CD8 T cells in Qa-1-deficient mice. *Nat Immunol*. 2004;5:516–523. doi: 10.1038/ni1063.
19. Hu YL, Metz DP, Chung J, Siu G, Zhang M. B7RP-1 blockade ameliorates autoimmunity through regulation of follicular helper T cells. *J Immunol*. 2009;182:1421–1428.
20. Choi YS, Kageyama R, Eto D, Escobar TC, Johnston RJ, Monticelli L, Lao C, Crotty S. ICOS receptor instructs T follicular helper cell versus effector cell differentiation via induction of the transcriptional repressor Bcl6. *Immunity*. 2011;34:932–946. doi: 10.1016/j.immuni.2011.03.023.
21. Ansel KM, Ngo VN, Hyman PL, Luther SA, Förster R, Sedgwick JD, Browning JL, Lipp M, Cyster JG. A chemokine-driven positive feedback loop organizes lymphoid follicles. *Nature*. 2000;406:309–314. doi: 10.1038/35018581.
22. Kuchen S, Robbins R, Sims GP, Sheng C, Phillips TM, Lipsky PE, Ettinger R. Essential role of IL-21 in B cell activation, expansion, and plasma cell generation during CD4+ T cell-B cell collaboration. *J Immunol*. 2007;179:5886–5896.
23. Yu B, Barbalic M, Brautbar A, Nambi V, Hoogeveen RC, Tang W, Mosley TH, Rotter JI, deFilippi CR, O'Donnell CJ, Kathiresan S, Rice K, Heckbert SR, Ballantyne CM, Psaty BM, Boerwinkle E; CARDIoGRAM Consortium. Association of genome-wide variation with highly sensitive cardiac troponin-T levels in European Americans and blacks: a meta-analysis from Atherosclerosis Risk in Communities and Cardiovascular Health studies. *Circ Cardiovasc Genet*. 2013;6:82–88. doi: 10.1161/CIRCGENETICS.112.963058.
24. Lenk GM, Tromp G, Weinsheimer S, Gatalica Z, Berguer R, Kuivaniemi H. Whole genome expression profiling reveals a significant role for immune function in human abdominal aortic aneurysms. *BMC Genomics*. 2007;8:237. doi: 10.1186/1471-2164-8-237.
25. Ait-Oufella H, Salomon BL, Potteaux S, Robertson AK, Gourdy P, Zoll J, Merval R, Esposito B, Cohen JL, Fisson S, Flavell RA, Hansson GK, Klatzmann D, Tedgui A, Mallat Z. Natural regulatory T cells control the development of atherosclerosis in mice. *Nat Med*. 2006;12:178–180. doi: 10.1038/nm1343.
26. Caligiuri G, Rudling M, Ollivier V, Jacob MP, Michel JB, Hansson GK, Nicoletti A. Interleukin-10 deficiency increases atherosclerosis, thrombosis, and low-density lipoproteins in apolipoprotein E knockout mice. *Mol Med*. 2003;9:10–17.
27. Lievens D, Habets KL, Robertson AK, Laouar Y, Winkels H, Rademakers T, Beckers L, Wijnands E, Boon L, Mosaheb M, Ait-Oufella H, Mallat Z, Flavell RA, Rudling M, Binder CJ, Gerdes N, Biessen EA, Weber C, Daemen MJ, Kuiper J, Lutgens E. Abrogated transforming growth factor beta receptor II (TGFβRII) signalling in dendritic cells promotes immune reactivity of T cells resulting in enhanced atherosclerosis. *Eur Heart J*. 2013;34:3717–3727.
28. Subramanian M, Thorp E, Hansson GK, Tabas I. Treg-mediated suppression of atherosclerosis requires MYD88 signaling in DCs. *J Clin Invest*. 2013;123:179–188. doi: 10.1172/JCI64617.
29. Caligiuri G, Khallou-Laschet J, Vandaele M, Gaston AT, Delignat S, Mandet C, Kohler HV, Kaveri SV, Nicoletti A. Phosphorylcholine-targeting immunization reduces atherosclerosis. *J Am Coll Cardiol*. 2007;50:540–546. doi: 10.1016/j.jacc.2006.11.054.
30. Caligiuri G, Nicoletti A, Poirier B, Hansson GK. Protective immunity against atherosclerosis carried by B cells of hypercholesterolemic mice. *J Clin Invest*. 2002;109:745–753. doi: 10.1172/JCI7272.
31. Baumjohann D, Preite S, Reboldi A, Ronchi F, Ansel KM, Lanzavecchia A, Sallusto F. Persistent antigen and germinal center B cells sustain T follicular helper cell responses and phenotype. *Immunity*. 2013;38:596–605. doi: 10.1016/j.immuni.2012.11.020.
32. Thaunat O, Field AC, Dai J, Louedec L, Patey N, Bloch MF, Mandet C, Belair MF, Bruneval P, Meilhac O, Bellon B, Joly E, Michel JB, Nicoletti A. Lymphoid neogenesis in chronic rejection: evidence for a local humoral alloimmune response. *Proc Natl Acad Sci USA*. 2005;102:14723–14728. doi: 10.1073/pnas.0507223102.
33. Thaunat O, Graff-Dubois S, Brouard S, Gautreau C, Varthaman A, Fabien N, Field AC, Louedec L, Dai J, Joly E, Morelon E, Soulillou JP, Michel JB, Nicoletti A. Immune responses elicited in tertiary lymphoid tissues display distinctive features. *PLoS One*. 2010;5:e11398. doi: 10.1371/journal.pone.0011398.
34. Thaunat O, Graff-Dubois S, Fabien N, Duthey A, Attuil-Audenis V, Nicoletti A, Patey N, Morelon E. A stepwise breakdown of B-cell tolerance occurs within renal allografts during chronic rejection. *Kidney Int*. 2012;81:207–219. doi: 10.1038/ki.2011.317.
35. Takemura S, Klimiuk PA, Braun A, Goronzy JJ, Weyand CM. T cell activation in rheumatoid synovium is B cell dependent. *J Immunol*. 2001;167:4710–4718.
36. Lacolley P, Regnault V, Nicoletti A, Li Z, Michel JB. The vascular smooth muscle cell in arterial pathology: a cell that can take on multiple roles. *Cardiovasc Res*. 2012;95:194–204. doi: 10.1093/cvr/cvs135.

CLINICAL PERSPECTIVE

B cells can modulate the development of atherosclerotic plaques. Their maturation into antibody-secreting cells is determined by T follicular helper cells. Here, we show that newly identified $CD8^+$ T regulatory cells control the activity of T follicular helper and B cells and consequently atherogenesis. We have identified the adventitial layer as a critical location for atherosclerosis-associated immune activity. Indeed, we show that lymphoid aggregates develop around human atherothrombotic arteries, particularly aortas affected by atherothrombotic aneurysms, are enriched in T follicular helper and B cells, and release immune effectors. Using mouse models, we demonstrate that disrupting the T follicular helper–B-cell axis with an anti-ICOSL antibody is a strategy that suppresses the formation of lymphoid aggregates around diseased arteries. Importantly, the use of this strategy also limits lesion development. Given the specificity of action of anti-ICOSL antibodies, they are good candidates for human translational trials. Indeed, they are currently being tested in lupus patients (http://www.ClinicalTrials.gov; NCT00774943). This approach could be considered to stop aneurysm progression.

SUPPLEMENTAL MATERIAL

Supplemental Methods

Human tissues

AAA tissues were obtained from patients undergoing surgery and enrolled in the RESAA protocol (REflet Sanguin de l'evolutivité des Anevrysmes de l'aorte abdominale). All patients gave informed written consent, and the protocol was approved by the Comite Consultatif de Protection des Personnes dans la Recherche Biomédicale (CCPRB, Paris-Cochin, approval no. 2095). Control aortas were sampled from dead organ donors with the authorization of the French Biomedicine Agency (PFS 09-007). These control aortic samples were non-aneurysmal (N-AA), devoid of thrombus but could present atheromatous lesions.

Mice

ApoE° mice were purchased from the Jackson Laboratory. The generation of the Qa1° and D227K ($Qa1^{D227K/D227K}$) mice was described previously [1, 2]. All mice were maintained on a C57BL/6J background and had a $Qa\text{-}1^{b}$ haplotype. The Qa1° and D227K mice were crossed with the ApoE° mice. The heterozygous offspring were then intercrossed to generate homozygous ApoE°-Qa1° and ApoE°-D227K mice. All animals were maintained on a regular chow diet and handled in accordance with European Union directives (86/609/EEC) on the care and use of laboratory animals in our facility. For each experiment, the mice were sacrificed by exsanguination under anesthesia (intraperitoneal injection of 100 mg/kg ketamine-HCL and 20 mg/kg xylazine). The experimental protocol was approved by the Animal Ethics Committee of the Institut National de la Santé et de la Recherche Médicale and was therefore performed in accordance with the ethical standards laid down in the 1964 Declaration of Helsinki and its later amendments. Review and approval of the study was also obtained from the Comité d'Éthique Paris-Nord #121 (no. B 7518 03).

Analysis of the atherosclerotic lesion extent

The extent of atherosclerotic lesions was measured in oil red O-stained cryosections of mouse aortic roots, as previously described [3]. Images were captured on a Zeiss Axiovert 200 M inverted microscope. A program developed in Quips language (Leica) allowed for the quantification of the surface area of the lesion and the total surface area of the aorta.

Phenotypic analysis of the atherosclerotic plaques

Transverse cryosections (10 µm thick) of mouse aortic roots were fixed in 4% paraformaldehyde (PFA). The slides were pre-incubated in blocking solution [5% bovine serum albumin (BSA), 0.1% Fish Gelatin and 100 mM Glycine] for

30 minutes. The samples were then incubated overnight at 4°C with the following fluorochrome-coupled primary antibodies: rat anti-mouse IgM (polyclonal, DyLight649, Jackson ImmunoResearch) and rat anti-mouse IgG (polyclonal, rhodamine, Jackson ImmunoResearch) or with the following purified primary antibodies: rat anti-mouse CD68 (clone FA-11, Serotec), rabbit anti-mouse α-SMA (polyclonal, Abcam), and goat anti-mouse VCAM-1 (polyclonal, R&D Systems). After several washes, the cryosections that were stained with the purified primary antibodies were incubated with the appropriate antibody (anti-rabbit TRITC; anti-rat DyLight649, Jackson ImmunoResearch) for 1 hour at room temperature (RT), and the slides were cover-mounted using Prolong Gold Antifade Reagent® (Invitrogen) for microscopy. To compare the plaque phenotypes between the different groups, we analyzed the ratio of the positively stained area (for each primary antibody) to the total lesion area.

Flow cytometry analysis

For mouse tissue analysis, the adventitial layer of the aorta, the inguinal and brachial lymph nodes, and the spleen were harvested for flow cytometry. The spleen and lymph nodes were disaggregated on a 70 µm filter to obtain a single cell suspension. Only results concerning the spleen are provided since those obtained with lymph node cells were redundant. The aorta was cut into small pieces and digested for 1 hour in 0.6 mg/mL Collagenase P (Roche), 2.4 mg/mL Dispase (Roche) and 0.3 mg/mL (Roche) in DMEM media at 37°C under constant shaking, as previously described [4]. A cell suspension from the peritoneum was obtained by peritoneal lavage with 5 mL of ice-cold PBS. After several washes with PBS, the cells were incubated with an anti-CD16/32 (Fc block, BD Biosciences) for 15 minutes at RT. The cells were washed and incubated for 30 minutes at 4°C with the antibodies described in Supplemental Table II. After an extensive wash, the cells were analyzed by flow cytometry. For the quantification of intracellular cytokines, the cells were incubated in 200 ng/mL phorbol-myristate-acetate (PMA, Sigma) and 500 ng/mL ionomycin (Sigma) in 24-well plates (10^6 cells/well) for 4 hours at 37°C, and Golgi Stop (1/1500, BD Biosciences) was added for the last 2 hours of the incubation. After several washes, the cells were stained for surface molecules, followed by fixation, permeabilization, and intracellular staining with the mouse Th1/Th2/Th17 phenotyping kit (BD Biosciences) according to the manufacturer's instructions. For the analysis of $CD4^+$ Tregs and for KI-67 and Bcl6 staining, the mouse regulatory T cell staining kit (eBioscience) was used according to the manufacturer's instructions.
For human tissue analysis, adventitial layer samples from the AAA and N-AA subjects were weighed, cut into small pieces (<1 mm) and digested using a previously described protocol [4]. After a wash step, the cells were stained with the antibodies described in Supplemental Table II.
Flow cytometry analysis was performed using an LSR II flow cytometer (BD Biosciences), and fluorescence activated cell sorting was performed with an ARIA III cell sorter (BD Biosciences). Data were analyzed with DIVA (BD Biosciences) and FlowJo (TreeStar) software.

Analysis of spleen GCs

Cryosections (10 µm thick) of mouse spleens were fixed in 4% PFA. The slides were incubated with avidin/biotin blocking solution (Dako) for 20 minutes and Mouse-on-Mouse Ig blocking solution (Vector) for 1 hour. The slides were then incubated with primary antibody (biotinylated mouse anti-mouse IgD, clone 217-170, BD Biosciences; rat anti-mouse GL7, clone Gl7, eBioscience) for 1 hour at 37°C. After several washes, the samples were incubated with the appropriate secondary antibody (TRITC-conjugated goat-rat IgG, polyclonal, Jackson ImmunoResearch; Alexa Fluor 647 streptavidin A647, Life Technologies) for 45 minutes at RT, and the slides were cover-mounted using Prolong Gold Antifade Reagent® (Invitrogen) for microscopy. For quantitative analysis, the GC density was calculated as follows: GL7-positive area*100/IgD-positive area.

Whole mount immunofluorescence staining of the mouse aortic adventitia

The mouse aortic adventitia was separated from the medial tube using binoculars and then processed as described previously [5]. Briefly, the adventitia was fixed in 4% PFA overnight and permeabilized with 0.6% Triton for 2 hours at RT. Purified rat anti-mouse B220 (RA3-6B2, BD Biosciences), isolectin B4 (Vector Laboratories) and primary hamster anti-mouse Gp38 (polyclonal, Angiobio) were used to stain the adventitia. After several washes, the adventitia was incubated with the appropriate secondary antibody (polyclonal rabbit anti-hamster DyLight488; goat anti-rat DyLight649, Jackson Immunoresearch) for 1 hour at RT, and the slides were cover-mounted using Prolong Gold Antifade Reagent® (Invitrogen) for microscopy.

Adoptive transfer of $CD4^+$ T cells

Spleens were harvested from 8-week-old ApoE° or ApoE°-D227K° (n=10/group) male mice and meshed through a 70 µm cell strainer (BD Biosciences). The resultant cell suspensions were processed for $CD4^+$ T cell purification using the CD4 T Lymphocyte Enrichment Set (BD Biosciences) according to the instructions of the manufacturer. The $CD4^+$ T cell purity and phenotype were analyzed by flow cytometry. The $CD4^+$ T cells were 85% pure in each preparation and displayed the same activation phenotype (CD62L, CD44, CD25) in each group. Male ApoE° recipient mice (n=9-10/group, 15 weeks old) received 2 injections of the purified $CD4^+$ T cells (10^7 cells/mouse/injection), 10 weeks apart. The mice were sacrificed at 35 weeks of age.

Adoptive transfer of $CD8^+$ Tregs

Under sterile conditions, spleens and lymph nodes (inguinal, axillary, brachial) were harvested from ApoE° mice (females, 8 weeks old, n=10) and meshed through a 70 µm cell strainer to obtain cell suspensions in PBS. The $CD8^+$ T cells were stained to perform a FACS-based purification to obtain fractions enriched in memory ($CD44^+CD122^-$) and $CD8^+$ Tregs ($CD44^+CD122^+$). The

antibodies used were: anti-mouse CD8 PerCP (clone 53-6.7, BD Biosciences), anti-mouse CD44 APC (clone IM7, BD Biosciences), and anti-mouse CD122 PE (clone TM-□1, BD Biosciences). After purification, the cells were extensively washed with sterile PBS and stained with Cell Trace violet tracker (Invitrogen), and $3x10^5$ cells from each preparation were injected into 35-week-old ApoE° mice (n=3/group). After 8 days, the mice were sacrificed, and their spleen cells were analyzed for the presence of the injected $CD8^+$ T cells and for the phenotypes of the $CD4^+$ T cell subsets.

Anti-ICOS ligand antibody treatment

Fifteen-week-old ApoE° and ApoE°-D227K mice (n=10 mice/group) received a weekly i.p. injection of 100 µg anti-ICOSL antibody (clone HK5.3, rat IgG2a anti-mouse) or isotype control (BioXcell). After 10 weeks of treatment, the mice were euthanized, blood samples were collected by puncture to obtain plasma, their hearts were frozen for analysis of aortic root lesions, their adventitias were dissected for TLO analysis, and their spleens were used for flow cytometry analysis and cryosections.

Immunohistochemistry on human samples

Human AAA and N-AA tissues were fixed in 4% PFA, embedded in paraffin and sectioned at 6 µm. The sections were deparaffinized in toluene, hydrated in ethanol and incubated in retrieval reagent (R&D Systems) for 20 minutes. After blocking in 5% BSA, the slides were incubated with purified primary antibody (mouse anti-human CD20, clone L-26; rabbit anti-human CD3, polyclonal, Dako; rat anti-human PNAd, MECA-79, BD Biosciences; rat anti-human Gp38, clone NZ-1, Angiobio; goat anti-human CXCL13, polyclonal, R&D Systems; rabbit anti-human CD21, clone EP3093, Abcam) or fluorochrome-coupled primary antibody (rat anti-human AICDA Alexa Fluor 488, clone 911, Abcam) overnight at 4°C. After several washes with PBS, the slides that were stained with the purified primary antibodies were incubated with the appropriate secondary antibody (polyclonal goat anti-rabbit DyLight649; goat anti-mouse rhodamine; goat anti-rat rhodamine; donkey anti-mouse rhodamine, Jackson Immunoresearch) at RT for 30 minutes and then cover-mounted using Prolong Gold Antifade Reagent® (Invitrogen) for microscopy.
The resulting fluorescence was detected with a Zeiss Axiovert 200 M microscope equipped with an AxioCam MRm version 3 camera, an ApoTome® system and AxioVision® image capture software.

Gene expression analysis

Total RNAs were extracted from cells sorted from human aortas using the TRIzol® reagent, and mRNA reverse transcription was performed using iScript reverse transcriptase (BioRad).
Real time quantitative PCR (RT-qPCR) was performed on a CFX 100 thermocycler (BioRad) using the primers listed Supplemental Table I. One nanogram of cDNA from each sample was mixed with forward and reverse primers (250 nM) and SYBR Green master mix (Qiagen) in a total reaction volume of 22 µL. The amplification program was as follows: 1 cycle at 50°C

for 2 minutes; 1 cycle at 95°C for 15 minutes; and 50 cycles at 95°C for 40 sec and 60°C for 1 minute. The data were analyzed using the $2^{-\Delta\Delta Ct}$ Pfaffl formula [6], and the Ct values of the genes of interest were normalized to the Ct values of β-actin (primers sequences are listed in Supplemental Table III). Clustering classification was performed using JMP9.

Biochemical analysis of mouse blood samples

To determine the total blood cell count in the mouse blood samples, fresh EDTA-anticoagulated blood samples were harvested from sacrificed mice and analyzed on a Vet ABC analyzer. The plasma was then separated by centrifugation at 2000 g for 15 minutes, and the plasma cholesterol and high-density lipoprotein (HDL) concentrations were measured using Infinity® Cholesterol-Liquid reagents and an Olympus AU-400 multiparametric analyzer. The data for the blood cell counts and lipid concentrations are displayed in Supplemental Table I.

Statistical analysis

Statistical analyses were performed using the JMP9 and Prism software programs. We used Student's t-tests or two-way ANOVA tests followed by Tukey's post-hoc tests when values were normally distributed, or non-parametric Mann-Whitney tests when it was not the case or when population size was too small ($n<8$), as specified in the figure legends.

Supplemental Figure Legends

Supplemental Figure 1

(**A**) Immunoglobulin titers in 8- (n=7), 15- (n=8), and 35- (n=6) week-old ApoE° mice (**B**) Splenic memory ($CD44^{high}CD122^{-}$; blue) and regulatory ($CD44^{high}CD122^{+}$; green) $CD8^{+}$ T cells from 8-week-old ApoE° mice were sorted by FACS, and the purity of the sorted cell suspensions was analyzed (bottom panels). (**C**) Flow cytometry analysis of Qa-1 expression by $CD4^{+}$ T cells with a naïve ($CD44^{low}CD62L^{+}$), memory ($CD44^{high}CD62L^{-}$), regulatory ($CD25^{high}CD62L^{-}CTLA4^{high}$), or Tfh ($CD44^{high}CXCR5^{high}PD\text{-}1^{high}$) phenotype performed on splenocytes from 35-week-old ApoE° mice (n=3). (**D**) The upper graphs show the quantification of the percentage of the $CD68^{+}$, IgM^{+}, and IgG^{+} areas in the lesions of 35-week-old ApoE° (n=6) and ApoE°-D227K (n=6) mice. The pictures below are representative immunofluorescence images of aortic root cryosections from 35-week-old ApoE° and ApoE°-D227K mice that were stained for αSMA (green) and VCAM (purple). The white boxes represent the areas that are magnified in the right panels. (Scale bar: 500 µm). (**E**) Quantification of oil red O-stained aortic root atherosclerotic lesions from 8-week-old ApoE° (n=12), ApoE-Qa1° (n=7) and ApoE°-D227K (n=16) mice or entire aortas (en-face staining) from 15-week-old ApoE° (n=3) and ApoE°-D227K (n=4) mice and from 35-week-old ApoE° (n=4) and ApoE°-D227K (n=4) mice. *|p<0.05; **|p<0.01; ***|p<0.001; Mann-Whitney test (A, D, E right) and two-way ANOVA (E left).

Supplemental Figure 2

(**A**) Quantification and (**B**) representative plots from the flow cytometry analysis of Bcl6 expression by splenic $CD4^{+}$ Tfh ($ICOS^{+}CXCR5^{+}$), non-Tfh ($ICOS^{+}CXCR5^{-}$) cells, and B cells from 35-week-old ApoE° (n=6) and ApoE°-D227K (n=4) mice (MFI: mean fluorescence intensity; n= 4-6 mice/group). (**C**) Flow cytometry analysis of the percentage of $KI\text{-}67^{+}$ cells among the Tfh ($CD44^{high}ICOS^{+}CXCR5^{+}$) cell population in the spleens of 35-week-old ApoE° and ApoE°-D227K mice (n= 4-6 mice/group). Flow cytometry analysis (**D**) of splenic plasma cells ($CD19{+}CD138^{+}IgD^{-}$) and (**E**) of the B-1a ($CD19^{+}B220^{low}CD23^{-}CD11b^{+}CD5^{+}$), B-1b ($CD19^{+}B220^{low}CD23^{-}CD11b^{+}CD5^{-}$), and B-2 ($CD19^{+}B220^{high}CD23^{+}$) B cells (among $CD45^{+}$ cells) in the peritoneal cavities of ApoE° and ApoE°-D227K mice (n= 4-6 mice/group). *|p<0.05; **|p<0.01; ***|p<0.001; Mann-Whitney test (A, C) and two-way ANOVA (D, E).

Supplemental Figure 3

(**A**) Total splenocytes from 8-week-old ApoE° and ApoE°-D227K mice were prepared for $CD4^{+}$ T cell enrichment. The suspensions of purified $CD4^{+}$ T cells were analyzed by flow cytometry for the percentages of total $CD4^{+}$ T cells with naïve ($CD44^{low}CD62L^{+}$), memory ($CD44^{high}CD62L^{-}$), or regulatory ($CD25^{high}$) phenotypes. (**B**) Quantification of the percentage of the $CD68^{+}$ and IgG^{+} areas within the aortic root atherosclerotic lesions of 35-week-old $CD4^{+}$ApoE°->ApoE° (n=7) and $CD4^{+}$ApoE°-D227K->ApoE° (n=9) mice. **|p<0.01; ***|p<0.001; Mann-Whitney test (B).

Supplemental Figure 4

(**A**) Quantification of the percentage of the $CD68^+$ and IgG^+ areas within the aortic root atherosclerotic lesions of 25-week-old ApoE° (n=5) and ApoE°-D227K (n=5) mice infused with anti-ICOSL or isotype control antibodies. (**B**) Percentages of $CD4^+ICOS^+PD\text{-}1^+$, $CD8^+CD44^{high}CD122^+$, and $CD8^+CXCR5^+Ly49^+$ cells (among $CD45^+$ cells) in the spleens of 25-week-old ApoE° (n=10) and ApoE°-D227K (n=10) mice infused with anti-ICOSL or isotype control antibodies. (**C**) Immunofluorescence of spleen cryosections from 25-week-old ApoE° and ApoE°-D227K mice infused with anti-ICOSL or isotype control antibodies. The cryosections were stained for IgD (green) and GL-7 (red). Arrowheads indicate the $GL\text{-}7^+$ areas within the B cell follicles. (Scale bar: 500 µm). *|p<0.05; **|p<0.01; ***|p<0.001; Two-way ANOVA with Tukey's post-hoc test (A, B).

Supplemental Figure 5

Flow cytometry analysis of the percentage of (**A**) B-1a ($CD19^+CD23^-CD5^+$), B-2 ($CD19^+CD23^+CD5^-$) and (**B**) GC ($B220^+CD95^{high}$) B cells (among L/D^- live $CD45^+$ cells) in the aortas of 40-week-old ApoE° mice (n=5; 2 experiments). The expression of CD11b, B220 and IgM is represented in the lower panels.

Supplemental Figure 6

From left to right: Representative 'en face' samples and hematoxylin-eosin staining of cross-sections of paraffin-embedded human aortas at early (top panels) and advanced (bottom panels) stages of atheroma. The dashed square represents the areas that are magnified on the right panels where serial sections were stained for CD20 (B cells; green), CD3 (T cells; red), PNAd (High Endothelial Venules; red), CXCL13 (red), CD21 (Follicular Dendritic cells; red), and nuclei (Hoechst, blue). (Scale bar: 50 µm).

Supplemental Figure 7

(**A**) Gating strategy for sorting naïve ($CD45RO^-$), memory ($CD45RO^+$), and regulatory ($CD25^{high}CD127^{low}$) $CD4^+$ T cells and Tfh cells for subsequent RT-qPCR analysis. Please note that neither PD-1 or ICOS staining was used in the gating strategy for the cell sorting, but they are displayed here to show that cells gated as Tfh cells (red) represent a cell population that is clearly distinct from the naïve, memory, and regulatory $CD4^+$ T cell populations. (**B**) The expression of T cell-related genes was determined by RT-qPCR on RNA extracted from purified cell-sorted naïve ($CD45RO^-$), memory ($CD45RO^+$), and regulatory ($CD25^{high}CD127^{low}$) $CD4^+$ T cells, and Tfh cells from aortic digests of human AAA tissues (n=9). The data were analyzed using the $2^{-\Delta\Delta Ct}$ Pfaffl formula [6], and the Ct values for the memory $CD4^+$ T cells, regulatory $CD4^+$ T cells, and Tfh cells were compared to the Ct values for the naïve cells. Importantly, the naïve phenotype of the reference cells does not preclude their possible stimulation within the inflamed tissue, which could modulate the expression of certain genes and generate heterogeneous gene expression profiles. The data were normalized to the Ct values for β-actin.

Supplemental Figure 8

Control of the Tfh-GC B cell axis by $CD8^+$ Treg cells. In untouched ApoE° mice, $CD8^+$ Treg cells control the Tfh cell population responsible for the generation of the GC-B cell response. The population of $CD8^+$ Treg cells decreases with disease progression, leading to an increase of the GC-B cell response. In D227K-ApoE° mice, Tfh cells are not anymore under the control of $CD8^+$ Treg cells. Consequently, the Tfh cell-dependent GC-B cell response is exaggerated in SLOs and in aortic TLOs, which leads to an accentuated atherosclerotis. The injection of anti-ICOSL antibody in ApoE°-D227K mice restored the control of the Tfh-GC B cell axis, and reduced the development of atherosclerosis.

References

1. Hu D, Ikizawa K, Lu L, Sanchirico ME, Shinohara ML, Cantor H. Analysis of regulatory cd8 t cells in qa-1-deficient mice. *Nature immunology*. 2004;5:516-523
2. Lu L, Kim HJ, Werneck MB, Cantor H. Regulation of cd8+ regulatory t cells: Interruption of the nkg2a-qa-1 interaction allows robust suppressive activity and resolution of autoimmune disease. *Proceedings of the National Academy of Sciences of the United States of America*. 2008;105:19420-19425
3. Nicoletti A, Kaveri S, Caligiuri G, Bariety J, Hansson GK. Immunoglobulin treatment reduces atherosclerosis in apo e knockout mice. *The Journal of clinical investigation*. 1998;102:910-918
4. Fletcher AL, Malhotra D, Acton SE, Lukacs-Kornek V, Bellemare-Pelletier A, Curry M, Armant M, Turley SJ. Reproducible isolation of lymph node stromal cells reveals site-dependent differences in fibroblastic reticular cells. *Frontiers in immunology*. 2011;2:35
5. Guedj K, Khallou-Laschet J, Clement M, Morvan M, Gaston AT, Fornasa G, Dai J, Gervais-Taurel M, Eberl G, Michel JB, Caligiuri G, Nicoletti A. M1 macrophages act as ltbetar-independent lymphoid tissue inducer cells during atherosclerosis-related lymphoid neogenesis. *Cardiovascular research*. 2014;101:434-443
6. Pfaffl MW. A new mathematical model for relative quantification in real-time rt-pcr. *Nucleic acids research*. 2001;29:e45

Supplemental Figure 1

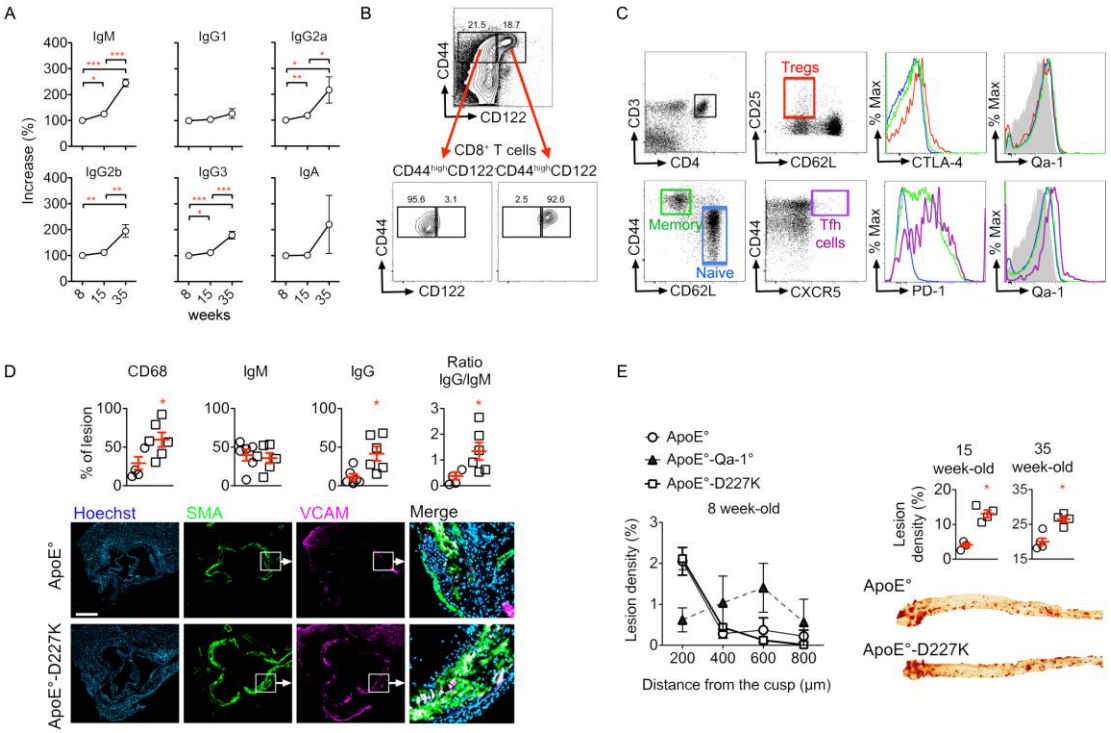

Supplemental Figure 2

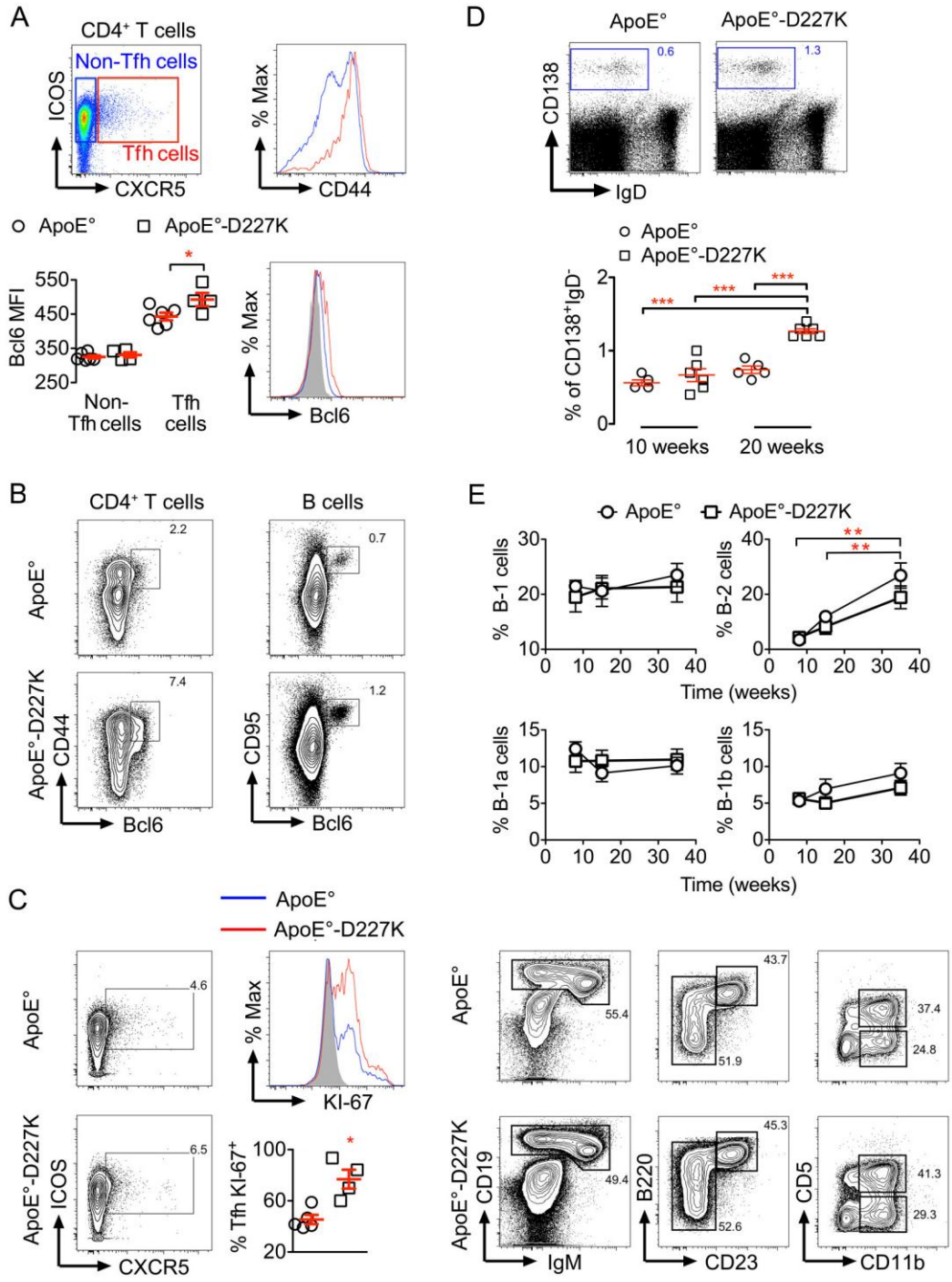

Supplemental Figure 3

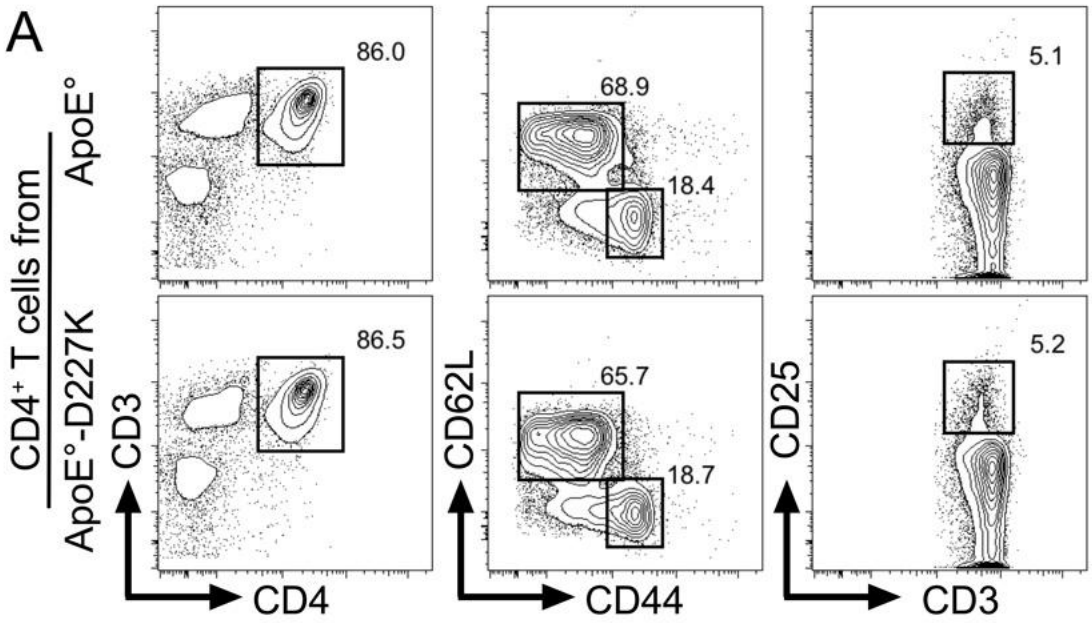

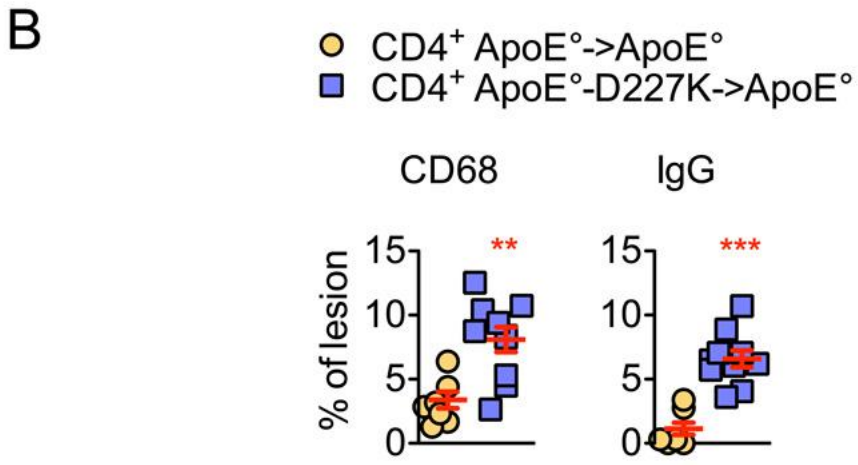

Supplemental Figure 4

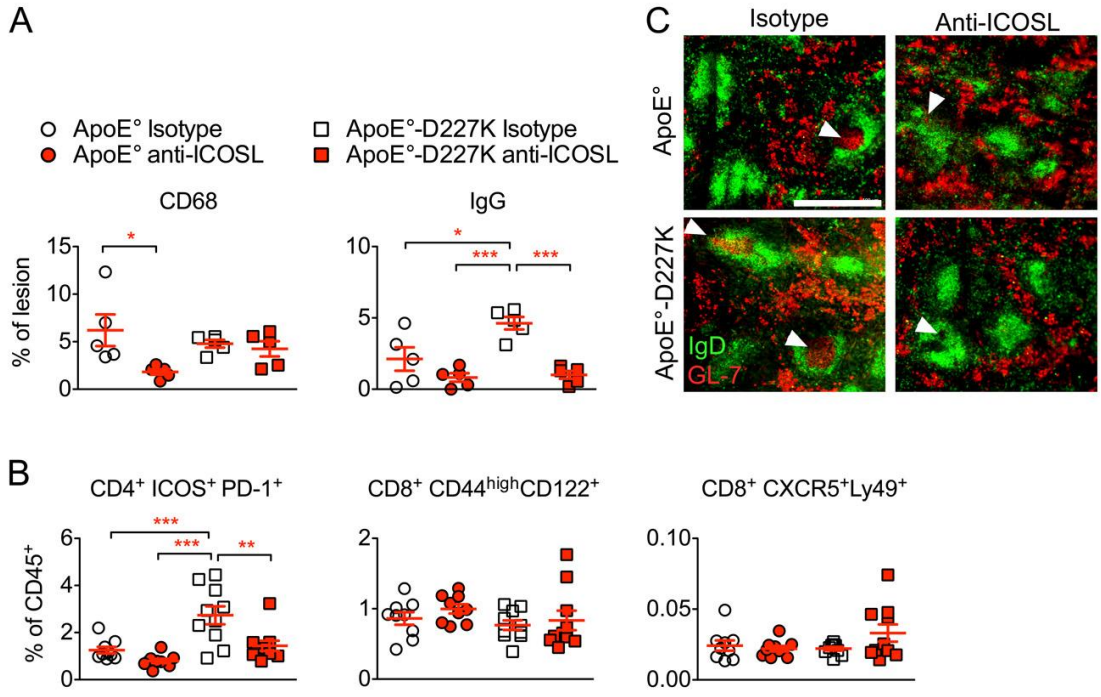

Supplemental Figure 5

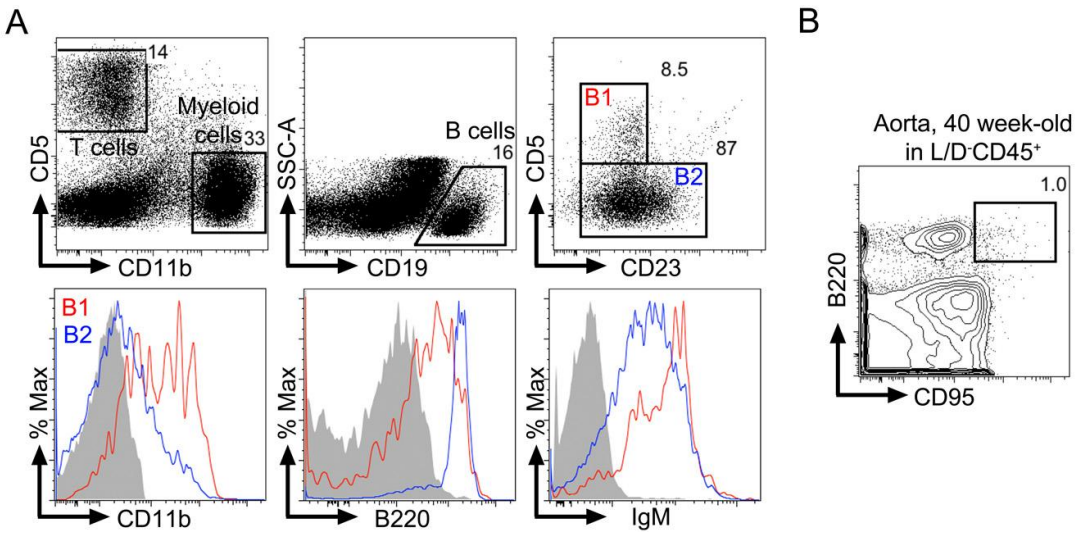

Supplemental Figure 6

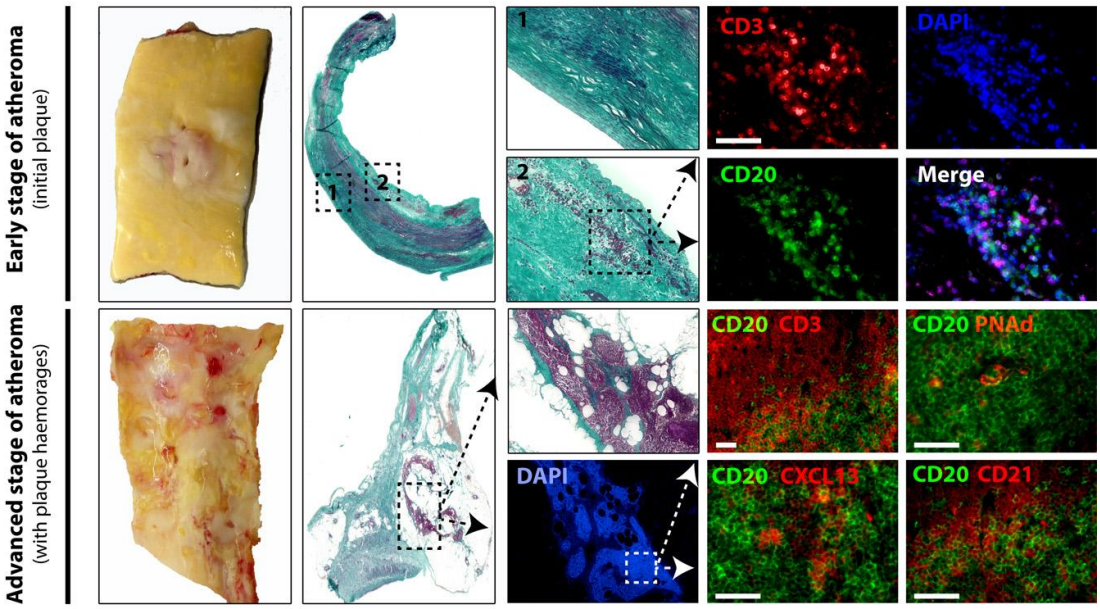

Supplemental Figure 7

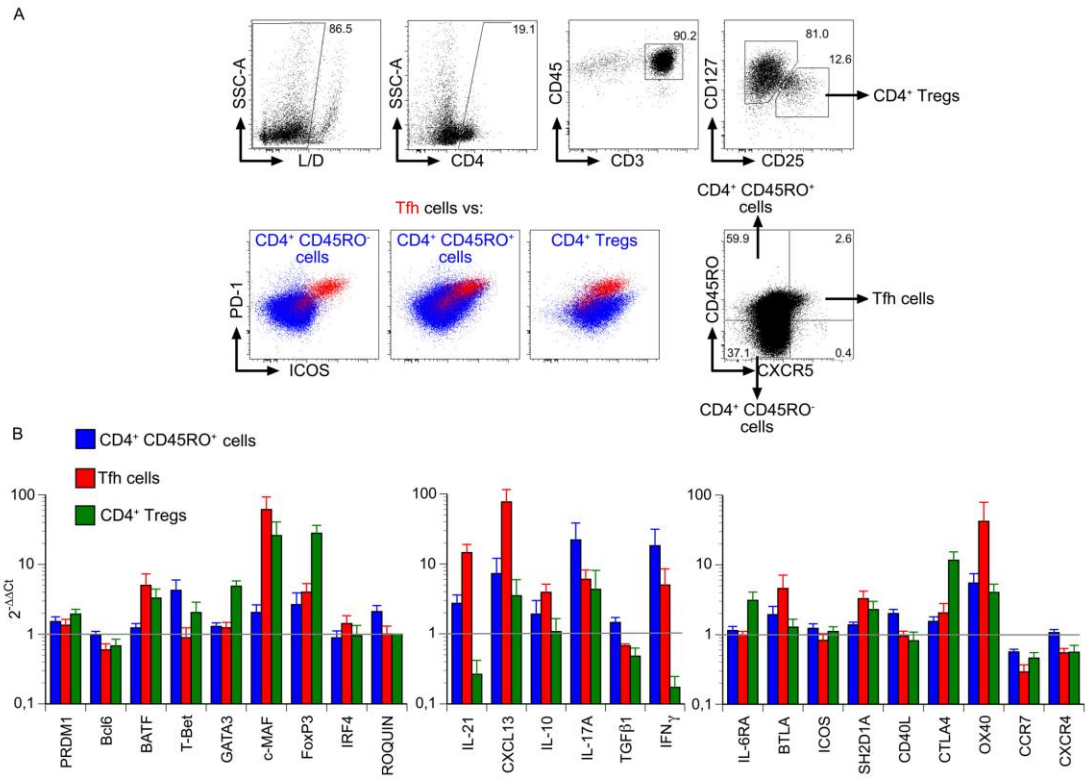

Supplemental Figure 8

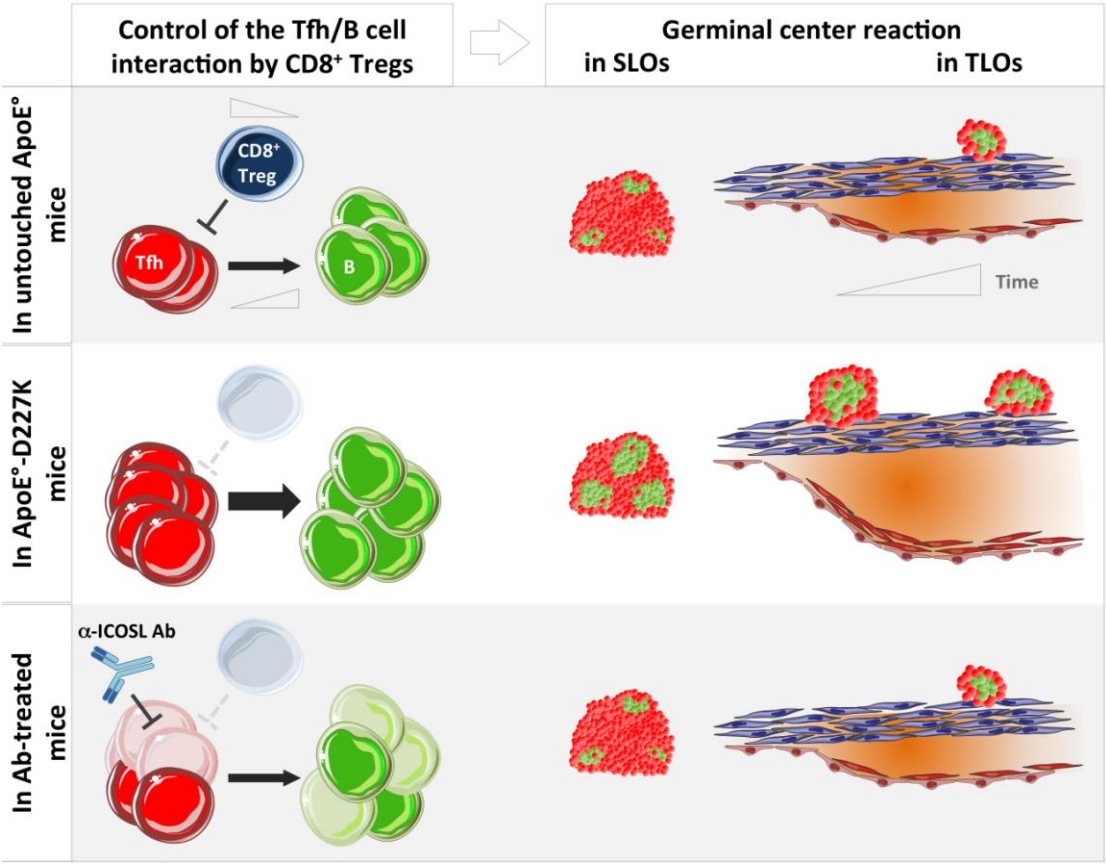

Supplemental Table 1

	Cholesterol and weight			Blood cell count (x1000 cells/µl)		
	HDL (mMol)	**Cholesterol** (mMol)	**Weight** (g)	**Lymphocytes**	**Monocytes**	**Granulocytes**
8 week-old						
ApoE°	0.968 ± 0.094	10.164 ± 0.671	22.7 ± 4.8	2.96 ± 0.21	0.20 ± 0.02	1.61 ± 0.18
ApoE°-Qa-1°	0.950 ± 0.042	10.170 ± 0.156	22.4 ± 2.9	2.55 ± 0.35	0.15 ± 0.07	1.22 ± 0.14
ApoE°-D227K	0.852 ± 0.110	8.768 ± 1.047	24.8 ± 4.4	2.59 ± 0.13	0.18 ± 0.02	1.38 ± 0.16
15 week-old						
ApoE°	1.140 ± 0.319	11.052 ± 1.787	28.1 ± 5.1	2.49 ± 0.16	0.19 ± 0.03	1.69 ± 0.21
ApoE°-Qa-1°	1.012 ± 0.151	7.200 ± 3.140	25.3 ± 3.9	2.02 ± 0.74	0.24 ± 0.09	1.24 ± 0.43
ApoE°-D227K	1.136 ± 0.281	11.672 ± 3.641	27.8 ± 3.5	2.58 ± 0.40	0.34 ± 0.09	1.93 ± 0.35
35 week-old						
ApoE°	0.756 ± 0.228	7.264 ± 3.585	27.9 ± 2.1	2.02 ± 0.12	0.17 ± 0.04	1.38 ± 0.26
ApoE°-Qa-1°	0.888 ± 0.228	8.596 ± 1.754	29.5 ± 3.6	2.11 ± 0.20	0.29 ± 0.06	1.90 ± 0.32
ApoE°-D227K	1.104 ± 0.119	11.684 ± 1.086	27.6 ± 3.2	2.23 ± 0.24	0.34 ± 0.10	1.98 ± 0.40
$CD4^+$ T cell transfer						
ApoE°-> ApoE°	1.228 ± 0.213	11.696 ± 2.861	33.5 ± 1.4	n.d	n.d	n.d
ApoE°-D227K ->ApoE°	1.352 ± 0.164	13.984 ± 1.357	33.3 ± 2.5	n.d	n.d	n.d
anti-ICOSL Ab treatment						
ApoE° isotype	1.168 ± 0.091	11.980 ± 1.093	24.2 ± 1.7	1.94 ± 0.46	0.11 ± 0.09	1.11 ± 0.44
ApoE° anti-ICOSL	1.200 ± 0.126	11.808 ± 1.288	23.9 ± 2.0	2.55 ± 0.70	0.12 ± 0.08	1.07 ± 0.53
ApoE°-D227K isotype	1.052 ± 0.206	11.408 ± 0.831	26.0 ± 2.4	1.60 ± 0.43*	0.11 ± 0.07	0.83 ± 0.45
ApoE°-D227K anti-ICOSL	1.128 ± 0.155	11.048 ± 1.869	24.7 ± 2.0	2.31 ± 1.00	0.14 ± 0.05	0.94 ± 0.33

Measurements were performed on five randomly selected mice per group

*$p<0.05$ between ApoE°-D227K-isotype vs ApoE° anti-ICOSL and ApoE°-D227K anti-ICOSL (two-way ANOVA). n.d.: not determined.

Supplemental Table 2

Panel	Antibody	Clone	Conjugate(s)	Reactivity	Source
Tfh cells (1)	Rat anti-CD3	172A	Alexia Fluor 700	Mouse	BD Bioscience
	Rat anti-CD4	GK1.5	APC-H7	Mouse	BD Bioscience
	Rat anti-CD8	53-6.7	PerCP	Mouse	BD Bioscience
	Rat anti-CD62L	MEL-14	FITC	Mouse	BD Bioscience
	Rat anti-CD44	IM7	APC	Mouse	BD Bioscience
	Hamster anti-PD-1	J43	Brillant Violet 421	Mouse	BD Bioscience
	Rat anti-ICOS	72.17G9	PE	Mouse	BD Bioscience
	Rat anti-CXCR5	2g8	PE-Cy7	Mouse	BD Bioscience
Tfh cells (2)	Rat anti-CD4	GK1.5	APC-H7	Mouse	BD Bioscience
	Rat anti-CD44	IM7	APC	Mouse	BD Bioscience
	Rat anti-CXCR5	2g8	PE-Cy7	Mouse	BD Bioscience
	Rat anti-ICOS	72.17G9	Biotinylated	Mouse	BD Bioscience
	Mouse anti-Bcl6	IG191/A8	PE	Mouse	Biolegend
	Rat anti-KI-67	16A8	PE	Mouse	Biolegend
B cells	Rat anti CD45R (B220)	RA3-682	Alexia Fluor 700	Mouse	BD Bioscience
	Hamster anti-CD95	JO2	PE-Cy7	Mouse	BD Bioscience
	Rat anti-IgM	R6-60.2	Brillant Violet 421	Mouse	BD Bioscience
	Rat anti-CD21	7G6	PE	Mouse	BD Bioscience
	Rat anti-CD23	B3B4	FITC	Mouse	BD Bioscience
CD8 regulatory T cells	Rat anti-CD4	GK1.5	APC-H7	Mouse	BD Bioscience
	Rat anti-CD8	53-6.7	PerCP	Mouse	BD Bioscience
	Rat anti-CD44	IM7	APC	Mouse	BD Bioscience
	Rat anti-CD122	TM-beta1	PE	Mouse	BD Bioscience
	Hamster anti-Ly-49	14B11	FITC	Mouse	eBioscience
	Rat anti-CXCR5	2g8	PE-Cy7	Mouse	BD Bioscience
B-1/B-2 cells	Rat anti-CD19	6D5	Brillant Violet 605	Mouse	Biolegend
	Rat anti-CD23	B3B4	FITC	Mouse	BD Bioscience
	Rat anti CD45R (B220)	RA3-682	Alexia Fluor 700	Mouse	BD Bioscience
	Rat anti-CD5	53-7.3	APC	Mouse	BD Bioscience
	Rat anti-CD11b	M1/70	PE	Mouse	BD Bioscience
Th1/Th17	Rat anti-CD3	172A	Alexia Fluor 700	Mouse	BD Bioscience
	Rat anti-CD4	GK1.5	APC-H7	Mouse	BD Bioscience
	Rat anti-IFNγ	XMG1.2	APC	Mouse	BD Bioscience
	Rat anti-IL-17	TC11-18H10	PE	Mouse	BD Bioscience
CD4 regulatory T cells	Rat anti-CD3	172A	Alexia Fluor 700	Mouse	BD Bioscience
	Rat anti-CD4	GK1.5	APC-H7	Mouse	BD Bioscience
	Rat anti-CD25	PC61	APC	Mouse	BD Bioscience
	Rat anti-FoxP3	FjK-16s	PE	Mouse	eBioscience
Tfh cells analysis	Mouse anti-CD45RO	UCHL1	Brillant Violet 785	Human	Biolegend
	Mouse anti CD45	HI30	eFluor 605	Human	eBioscience
	Mouse anti-CD8	RPA-TB	Alexia Fluor 700	Human	BD Bioscience
	Mouse anti-CD3	OKT3	eFluor 450	Human	eBioscience
	Mouse anti-ICOS	dx29	PE	Human	BD Bioscience
	Rat anti-CXCR5	rf8b2	FITC	Human	BD Bioscience
	Mouse anti-PD-1	EH1 2.1	PerCP-Cy5.5	Human	BD Bioscience
	Mouse anti-CD4	UCHL1	PE-CF594	Human	BD Bioscience
Tfh cells sorting	Mouse anti-CD3	OKT3	Brillant Violet 711	Human	Biolegend
	Mouse anti-CD4	RPA-T4	V450	Human	BD Bioscience
	Mouse anti-CD127	MB15-18C9	APC	Human	Milteny
	Mouse anti-CD25	M-A251	PE-Cy7	Human	BD Bioscience
	Rat anti-CXCR5	rf8b2	FITC	Human	BD Bioscience
	Mouse anti CD45	HI30	eFluor 605	Human	eBioscience
	Mouse anti-PD-1	EH1 2.1	PerCP-Cy5.5	Human	BD Bioscience
	Mouse anti-ICOS	dx29	PE	Human	BD Bioscience
	Mouse anti-CD45RO	UCHL1	Brillant Violet 785	Human	Biolegend
B cells	Mouse anti-CD19	HIB19	Brillant Violet 785	Human	Biolegend
	Mouse anti CD45	HI30	eFluor 605	Human	eBioscience
	Mouse anti-HLA-DR	L234	APC-H7	Human	BD Bioscience
	Mouse anti-CD27	M-T271	Brillant Violet 421	Human	BD Bioscience
	Mouse anti-IgD	IA6-2	APC	Human	BD Bioscience
	Mouse anti-CD38	HIT2	FITC	Human	BD Bioscience
	Mouse anti-CD95	DX2	FITC	Human	BD Bioscience

Supplemental Table 3

Genes	Forward primers	Reverse primers
ACTB	TCCCTGGAGAAGAGCTACGA	TTTCGTGGATGCCACAGGAC
IL10	GACTTTAAGGGTTACCTGGGTTG	TCACATGCGCCTTGATGTCTG
CTLA4	TGCAAGGTGGAGCTCATGTA	ACAGCTGTGAGGAGAAAGC
CXCL13	CAGCCTCTCTCCAGTCCAAG	TGAGGGTCCACACACACAAT
BTLA	ATGGGTCATACCGCTGTTC	CCTGGTGCTTGCTTCTGT
CCR7	AGGTATGCCTGTGTCAAGATGAGGT	CAGTAGGCCCACGAAACAAA
B3GAT1	GACGACGACAACACCTAC	GTCAAACACCGTCTTCCAG
CXCR4	GCCCACCATCTACTCCATC	TGTCCGTCATGCTTCTCA
ICOS	AAGTCAGGCCTCTGGTATTTCT	GCATAAAATTTGTACACCTCCGT
IFNG	AGACCATCAAGGAAGACAT	TGCTTTGCGTTGGACATTCA
IRF4	GACACACAGCAGTTCTTGTCAG	TGAGCTGTGATGAGCTTTCT
TNFRSF4	AAGTGGGAGTGAGCGGAA	CTCACAGATTGCGTCCGAG
RC3H1	GTATGTACCAGAATCCAGAGA	ATGAAAGGTAGGAGGCAA
TGFB1	GTGGAAACCCACAACGAAAT	CACGTGCTGCTCCACTTTTA
SH2D1A	GGCTGTGTATCATGGCAAAA	TGCTGTCTCAGCAGTCCAAGAA
BCL6	AACCTGAAAACCCACACTCG	TGACGGAAATGCAGGTTACA
MAF	TCGCCACATGATTAGAATGC	GCCTTCTGAAAGCAGGAAAA
IL6R	TCCTCTGCATTGCCATTGTTCT	TTGTGGCTCGAGGTATTGTC
TBX21	CCACCTGTTGTGGTCCAAGT	ACCACGTCCACAAACATCCT
BATF	ACAGCAGTGACTCCAGCTTC	CGGCAATACGATTTTTCTCC
IL17A	AGGAATCACAATCCCACGAA	TATCTCTCAGGGTCCTCATT
CD40LG	ATTGGGTCAGCACTTTTTGC	TTCACAAAGCCTTCAAACTGG
FOXP3	ACCTTCCCAAATCCCAGT	CACTTGCAGACACCATTTGC
GATA3	CTCATTAAGCCCAAGCGAAG	TCCTCCAGAGTGTGGTTGTG
PRDM1	GCAACAAGGGCTTTACTCA	GGCAGGGCACACCTTGCATTGGTAT
IL21	TCGCCACATGATTAGAATGC	AAGCAGGAAAAAGCTGACC

Control of the T Follicular Helper–Germinal Center B-Cell Axis by CD8$^+$ Regulatory T Cells Limits Atherosclerosis and Tertiary Lymphoid Organ Development

Marc Clement, Kevin Guedj, Francesco Andreata, Marion Morvan, Laetitia Bey, Jamila Khallou-Laschet, Anh-Thu Gaston, Sandrine Delbosc, Jean-Marc Alsac, Patrick Bruneval, Catherine Deschildre, Marie Le Borgne, Yves Castier, Hye-Jung Kim, Harvey Cantor, Jean-Baptiste Michel, Giuseppina Caligiuri and Antonino Nicoletti

Circulation. 2015;131:560-570; originally published online December 31, 2014;
doi: 10.1161/CIRCULATIONAHA.114.010988
Circulation is published by the American Heart Association, 7272 Greenville Avenue, Dallas, TX 75231

Print ISSN: 0009-7322. Online ISSN: 1524-4539